Developing a model for detailed simulations of the chemistry and aerosol microphysics of stratospheric volcanic injections with a focus on two case studies: the June 15th, 1991 eruption of Mount Pinatubo and the August 12th-15th eruption of Cerro Hudson

by

Parker Case

B.A., Columbia University, 2016

A thesis submitted to the

Faculty of the Graduate School of the

University of Colorado in partial fulfillment

of the requirement for the degree of

Doctor of Philosophy

Department of Atmospheric and Oceanic Sciences

2022

Committee Members:

Brian Toon

Charles Bardeen

Daven Henze

Peter Colarco

Jen Kay

Case, Parker (Ph.D., Atmospheric and Oceanic Sciences)

Developing a model for detailed simulations of the chemistry and aerosol microphysics of stratospheric volcanic injections with a focus on two case studies: the June 15th, 1991 eruption of Mount Pinatubo and the August 12th-15th eruption of Cerro Hudson

Thesis directed by Associate Professor Owen B. Toon

A version of the Goddard Earth Observing System (GEOS) has been developed for simulating dynamics and impacts of volcanic sulfate aerosols in the stratosphere. The GEOS-Chem chemistry module simulates the chemistry of the volcanic plume, using online oxidants and a detailed treatment of both the sulfur cycle and stratospheric ozone. Aerosol microphysics are simulated using the Community Aerosol and Radiation Model for Atmospheres (CARMA) sectional aerosol model. In this thesis, this model is described then applied to the case of stratospheric volcanic aerosols in 1991 from the June 15th Mount Pinatubo (15°N, 120°E) eruption and the August 15th Cerro Hudson (45°S, 72°W) eruption. The model is constrained by observations and applied to scientific questions about volcanic aerosols.

The 1991 eruption of Mount Pinatubo injected between 10 Tg and 20 Tg of SO_2 gas into the stratosphere, making it the largest volcanic injection of the satellite era. Modeling evidence shows that hydroxyl radical concentrations in the plume may have become depleted by 90% in the days following the eruption, slowing the initial oxidation of SO_2. Our model supports this hypothesis, showing the e-folding time for SO_2 increasing from a background value of 31 days to more than 200 days. Two months later, Cerro Hudson erupted 2.6 Tg SO_2 into the Southern midlatitudes. Modeling studies of Pinatubo have often neglected the Cerro Hudson eruption and attributed Southern Hemisphere observations of stratospheric aerosol in 1991 to transport of Pinatubo aerosols across the equator. The model developed here suggests that half of the optical depth in the Southern Hemisphere stratosphere in 1991 was a result of Cerro Hudson. Observations of volcanic aerosols and anomalously low ozone in the stratosphere above McMurdo Bay (77°S, 166°E) and South Pole Station in September and October 1991 suggest Cerro Hudson aerosols also impacted the 1991 ozone hole. Our model shows that Cerro Hudson may have decreased ozone by 26% between 15 km and 20 km by providing extra surface area for heterogeneous chemistry in September 1991. Additionally, the model shows that the radiative and dynamical impact of Cerro Hudson slowed ozone recovery between 20 km and 25 km.

CONTENTS

TABLES

Table

FIGURES

Figure

CHAPTER I

INTRODUCTION

1.1 Motivations and Science Questions

Particularly powerful volcanic eruptions can inject volcanic gasses and aerosols as high as the middle stratosphere, creating plumes with unique conditions in the relatively homogeneous stratosphere. The primary materials injected in these eruptions are volcanic ash, water vapor and sulfur dioxide gas. The majority of ash by mass is lost to sedimentation as the large particles settle quickly, within a couple weeks (Niemeier et al., 2009; Vernier et al., 2016), but numerous submicron ash particles may linger (Zhu et al, 2020). Water vapor will condense to form ice, which is also quickly removed by sedimentation, but may leave some vapor behind. The sulfur dioxide (SO_2) remains in the stratosphere and is oxidized by stratospheric oxidants, primarily hydroxyl radical (OH), where it is eventually turned into sulfuric acid gas which nucleates, along with water, to form sulfate aerosols (Hamill et al., 1997). These sulfate aerosols enhance the size and optical thickness of the background sulfate aerosols in the stratosphere, which are primarily a result of carbonyl sulfide (OCS) emissions from the surface of Earth's oceans (Crutzen et al., 1976; Turco et al., 1980; Brühl et al., 2012; Sheng et al., 2015) or from tropospheric aerosols lofted into the stratosphere by ascending air in the tropics. The

enhancement from these aerosols can be detected for months to years following the eruption, depending on the latitude, altitude, and magnitude of the injection.

These events have been shown to decrease temperature in the troposphere, increase temperature in the stratosphere, and cause a decrease in ozone concentration. The volcanic aerosol cools the troposphere by attenuating solar radiation. This effect is the most important factor in natural climate variability and caused a decrease in peak net radiative forcing of about 4 W/m2 and cooled the global troposphere by about 0.4 K for the largest events in the 20th century in the global temperature record (Thompson et al., 2009). Simultaneously, the aerosol increases the temperature of the stratosphere by absorbing terrestrial radiation and near infrared solar radiation, raising lower stratospheric temperatures (Randel et al., 2010). Finally, the additional aerosol surface area from these events can alter ozone chemistry by changing the microphysical properties of polar stratospheric clouds and by providing additional surface area for heterogeneous reactions important to the activation of ozone depleting substances. Volcanic eruptions have been shown to impact both midlatitude ozone as well as springtime ozone depletion (Aquila et al., 2013; Solomon et al., 2016; Stone et al., 2021).

Volcanic eruptions which impact the stratosphere are infrequent and diverse in latitude, altitude, composition, and season, meaning that each eruption impacts the composition and dynamics of the stratosphere differently. Satellite observations of volcanic SO_2 and aerosol have helped constrain the impact of historical eruptions. The largest eruption of the satellite record, the June 15th

eruption of Mount Pinatubo, injected between 10 and 20 Tg of SO_2 into the stratosphere. This eruption increased stratospheric aerosol optical depth (sAOD) and cooled the troposphere for 2-3 years. More recent satellite observations have shown the varying impact of smaller eruptions, including the February 13th, 2014 eruption of Kelud; the April 22nd, 2015 eruption of Calbuco; and the January 15th, 2022 eruption of Hunga Tonga. In-situ observations of stratospheric volcanic plumes are rare because of the altitude and infrequency of the events. In-situ measurements of aerosol size at specific locations have given insight into how volcanic eruptions impact the background stratospheric aerosol months to years after the eruption but often are not able to capture the early plume (Deshler et al., 2019).

These observational limitations mean that there are remaining uncertainties in the impact of these events. Because the largest eruptions can impact global temperatures and even modest eruptions can enhance ozone depletion, modeling these events is important to understanding historical temperature records, predicting future temperature trends, and monitoring the Antarctic ozone hole and boreal springtime ozone depletion. The 1991 eruption of Pinatubo, in particular, has been of particular importance in understanding the sensitivity of the climate system. More recent eruptions have also been posited to have deepened and widened the ozone hole during a time when it would be otherwise expected that the Antarctic ozone hole should be decreasing in severity

(Solomon et al., 2016; Stone et al., 2021).

1.2 Thesis Organization

In this thesis, I have focused on the June 15th, 1991, eruption of Mount Pinatubo and the August 12th-15th eruptions of Cerro Hudson. As part of this thesis I address several primary scientific questions: (i) What were the relative importance of the 1991 eruptions of Pinatubo and Cerro Hudson in the Southern Hemisphere in 1991? (ii) How did the initial injection of SO_2 from the 1991 eruption of Pinatubo impact stratospheric OH within the plume and what effect did this have on the formation and growth of the Pinatubo volcanic aerosol? (iii) How did the 1991 eruption of Cerro Hudson impact the 1991 ozone hole?

For this work, I developed a version of the NASA Goddard Earth Observing System (GEOS) model with a unique coupling between a sectional aerosol microphysics module (CARMA) and a tropospheric and stratospheric chemistry mechanism (GEOS-Chem). This model is specifically meant to combine a contemporary chemistry mechanism having online oxidants with a sectional approach to aerosol microphysics. In the first chapter, I will describe the model developments I made in order to construct an appropriate model to simulate these types of events. Additionally, chapter one includes a description of the model's simulation of the 1991 eruptions, focused on validating the model and addressing the first two science questions. The second chapter of this thesis is focused on the Cerro Hudson eruption, reconciling various observational records of the eruption,

and evaluating the possible impact of this eruption on the 1991 ozone hole. Chapter 1 has been submitted to the Journal of Advances in Modeling Earth Systems as Case et al. (2022a) and chapter 2 is planned to be submitted to Geophysical Research Letters as Case et al. (2022b). Additionally, an appendix is included describing the sectional aerosol model CARMA.

CHAPTER II

SIMULATIONS OF THE AEROSOL LAYER FROM THE 1991 ERUPTIONS OF MOUNT PINATUBO AND CERRO HUDSON WITH A NEW COUPLED SECTIONAL AEROSOL MICROPHYSICS AND CHEMISTRY MODEL IN THE NASA GEOS EARTH SYSTEM MODEL

2.1 Introduction

The June 15th, 1991, eruption of Mount Pinatubo in the Philippines triggered an important step forward in our understanding of how large volcanic eruptions impact the atmosphere and the broader climate system. This eruption caused the most extreme stratospheric aerosol optical depth (AOD) and the largest impact on global surface temperatures since we have had the capability to observe the atmosphere from satellites (Kovilakam et al., 2020; Santer et al., 2014). Because of this, Pinatubo is often used as a test case for atmospheric models and Earth system models (e.g. Aquila et al., 2012; Dhomse et al., 2014; Mills et al., 2017; and Sukhodolov et al., 2018).

These modeling studies, alongside analyses of satellite and ground-based observations have highlighted several ways in which volcanic eruptions of the magnitude of Mt. Pinatubo impact the Earth system. First, a significant decrease in lower tropospheric temperature was observed in the years following Pinatubo (Santer et al., 2014). Large tropical volcanic eruptions inject ash and sulfate aerosols alongside sulfur compounds, including sulfur dioxide (SO_2) and carbonyl sulfide (OCS). These compounds oxidize and nucleate into new sulfuric acid (H_2SO_4) particles or condense onto pre-existing aerosols, increasing the albedo of the Earth

(Dutton & Christy, 1992; Stenchikov et al., 1998; McCormick et al., 1995) and cooling its surface. The surface cooling observed after Pinatubo and other similarly large eruptions has inspired research into solar radiation management of climate via injection of aerosols into the stratosphere as a way to mitigate the warming caused by increasing greenhouse gas concentrations (e.g. Crutzen, 2006; Kravitz et al., 2017; MacMartin et al., 2017; Tilmes et al., 2017; Visioni et al., 2019).

In addition to surface cooling, the increased aerosol loading from volcanic eruptions leads to enhanced absorption of near-infrared and terrestrial longwave radiation and to a subsequent warming of stratospheric temperatures (Angell, 1997; Free & Lazante, 2009). Circulation changes due to this heating, alongside changes to heterogeneous chemistry and photochemistry, cause changes to global ozone chemistry (Kinne et al., 1992; Prather, 1992; Solomon, 1999; Bekki et al., 1993; Aquila et al., 2013; Dhomse et al., 2015). Volcanic aerosols that reach polar latitudes also contribute to enhanced spring-time ozone depletion and have been associated with years of anomalously severe ozone holes (Hofmann & Oltmans, 1993; Stone et al., 2017; Solomon et al., 2016; Zhu et al., 2018; Tabazadeh et al., 2002). This ozone depletion has been identified in the years 1992 and 1993 as the Pinatubo aerosol reached high Southern latitudes (Hofmann & Oltmans, 1993; Kerr, 1993; Knight et al., 1998;).

Despite the numerous studies on the 1991 eruption of Mt. Pinatubo (e.g. Santer et al., 2014; LeGrande & Anchukaitis, 2015; Yang et al., 2019), questions remain about the parameters of the eruption and how to represent it in global

models. For example, the estimated amount of the SO_2, sulfate, and ash injected varies widely across these studies. Additionally, Pinatubo was unique in the satellite record for its spread from the Northern tropics to the Southern Hemisphere shortly after the eruption (Pitari et al., 2016). These prior modeling studies have emphasized the importance of injection altitude in correctly modeling the transport of the Pinatubo plume (Timmreck et al., 1999; Aquila et al., 2012), but observations define a large range of plausible altitudes for the eruption (Holasek et al., 1996; Tupper et al., 2005). This uncertainty is due to sparse observations of the thick plume's vertical structure near the time of the eruption, in part caused by near-total attenuation of the sunlight observed by occultation measurements, as well as the confounding impacts of coincident meteorology, including Typhoon Yunya (Holasek et al., 1996). This leaves researchers to "tune" the injection height in simulations to compensate for a particular model's transport characteristics. Even so, the unique rapid spread of the Pinatubo aerosol into the Southern Hemisphere is challenging to re-create with global models. Multiple mechanisms have been proposed to explain this spread: the evaporation, transport, and condensation of sulfuric acid vapor above the plume (Dhomse et al., 2014); other uncertainties associated with the injection parameters of Pinatubo (e.g. magnitude, timing, and initial horizontal spread) (Niemeier et al., 2009); stratospheric dynamical changes due the radiative interaction of the volcanic sulfate (Dhomse et al., 2014); and the neglect of the August 15, 1991, Cerro Hudson eruption in most models (English et al., 2013).

Another uncertainty associated with modeling the Pinatubo plume in global models is whether the eruption altered the local oxidizing power of the atmosphere and how that impacted the conversion of SO_2 to aerosol. Early modeling studies of volcanic plumes in the stratosphere and observational estimates of the oxidation of the Pinatubo sulfur dioxide assumed the loss of OH due to its reaction with SO_2 to be negligible for a Pinatubo-sized eruption because of the short lifetime and constant production of the molecule in the stratosphere (McKeen et al., 1984; Bekki, 1995). More recently, however, Mills et al. (2016) showed, using a model with interactive oxidants, that OH can decrease by as much as 95% within the sulfur dense environment of the Pinatubo plume, slowing down the oxidation of SO_2 to sulfuric acid and sulfate aerosol.

In this study, we revisit the Pinatubo eruption using an updated version of the Goddard Earth Observing System (GEOS) Earth system model, now coupled with the aerosol sectional microphysics module Community Aerosol and Radiation Model for Atmospheres (CARMA) and the GEOS-Chem tropospheric and stratospheric chemistry mechanism. With respect to previous volcanic studies with the GEOS model (Aquila et al. 2012, 2013, 2021) this updated version includes, for the first time, a representation of the evolving volcanic aerosol size distribution in CARMA and a comprehensive chemistry mechanism in GEOS-Chem. This is, to our knowledge, the first simulation of the Pinatubo eruption performed with the GEOS-Chem mechanism.

Below we outline and evaluate the capabilities of this new model and use it to simulate the 1991 eruption of Pinatubo. The extensive literature around observing and modeling this eruption provide many ways to understand this novel model in the context of the observed eruption and prior modeling efforts. Secondarily, our ensemble of simulations can provide insight into the remaining uncertainties in the Pinatubo literature. We estimate the relative importance of transported Pinatubo aerosols and Cerro Hudson aerosols in Southern Hemisphere in 1991 and we explore the hypothesis that OH depletion slowed initial SO_2 oxidation rates in the Pinatubo plume.

2.2 Model Description

GEOS is an Earth System Model based on the architecture of the Earth System Modeling Framework (ESMF) (Hill et al., 2004; Molod et al., 2015). In this study, we use the atmospheric general circulation model (AGCM) configuration in its "free-running" mode; the model calculates its own meteorology without any data assimilation and with imposed sea surface temperatures based on observations. The GEOS system has been shown to perform well in stratospheric chemistry and transport processes (SPARC CCMVal, 2010; Strahan et al., 2011; Douglass et al., 2012). We run GEOS at a ~100 km horizontal resolution on a cubed-sphere grid with 72 hybrid-sigma vertical levels extending from the surface to ~80 km. While the GEOS AGCM can be coupled to various aerosol modules, here we are using the sectional aerosol microphysics from the Community Aerosol and Radiation Model

for Atmospheres (CARMA, Toon et al., 1988; Bardeen et al., 2008). In this work we have coupled CARMA to the GEOS-Chem tropospheric and stratospheric chemistry mechanism (Bey et al., 2001; acmg.seas.harvared.edu/geos/), and both CARMA and GEOS-Chem are radiatively interactive within the model.

CARMA is a sectional aerosol microphysics model that can be configured to simulate aerosols of many different types; past studies have used it to simulate sulfates, volcanic ash, dust, carbonaceous aerosols, and nitrates. CARMA was introduced in GEOS for application to dust (Colarco et al., 2014) and has subsequently been expanded to include sulfate aerosols (Chen et al., 2018). To fit the focus of this study, we have configured CARMA to simulate only sulfate aerosols. Sensitivity experiments have shown a sulfate simulation using 24 size bins, spread logarithmically in volume between 0.25 nm and 6.7 μm in radius reasonably represents the background stratospheric aerosol observed by in situ optical particle counter observations. CARMA simulates the nucleation, condensational growth and evaporation, coagulation, and settling of sulfate aerosols in our model, following the mechanism of English et al. (2013). Other aerosol species are calculated using the bulk aerosol microphysics package as part of GEOS-Chem and are not directly interactive with CARMA.

GEOS-Chem was originally a 3-D chemical transport model driven by assimilated meteorological data from the GEOS Earth system model and analysis system (Bey et al., 2001). It has since been implemented in the GEOS AGCM as a tropospheric and stratospheric chemistry mechanism (Hu et al., 2016; Keller et al.,

2021). GEOS-Chem's chemistry calculation is the most comprehensive chemistry mechanism in the GEOS framework and here we specifically take advantage of GEOS-Chem's interactive oxidants and sulfur cycle to simulate the chemistry of stratospheric volcanic plumes.

For this study, CARMA and GEOS-Chem have been coupled via the production and loss of sulfuric acid, aqueous aerosol production, and heterogeneous chemistry. This coupling is shown diagrammatically in Fig. 2.1. GEOS-Chem's chemistry mechanism tracks sulfuric acid/sulfate precursors (SO_2, OCS, etc.) and produces both gaseous sulfuric acid as well as aqueously produced sulfate, which are both passed to CARMA. In order to calculate the nucleation rate, condensation, and evaporation of sulfate aerosols, CARMA tracks the sulfuric acid vapor tracer. After its microphysics are calculated, CARMA provides GEOS-Chem with aerosol bulk mass and aerosol surface area for heterogeneous chemistry calculations and any loss and production of sulfuric acid vapor by condensation or evaporation on sulfate aerosols. This setup includes the advanced chemistry of GEOS-Chem, the detailed aerosol microphysics calculations of CARMA, and the heterogeneous chemistry calculations within GEOS-Chem using CARMA derived aerosol properties. The current version of this model uses the CARMA total mass but assumes a lognormal aerosol size distribution for the calculation of effective radius and optical properties in GEOS-Chem's photolysis codes. This approach to photolysis will be updated to use CARMA optical properties in a future version of

the model. The CARMA aerosols are fully radiatively interactive with the GEOS Earth system model, as are the GEOS-Chem gas phase species.

In addition to being the first time the GEOS model has been run using interactive sulfur chemistry and sectional aerosol microphysics, this is the first simulation we are aware of with the GEOS-Chem stratospheric chemistry mechanism applied to the Pinatubo eruption, and so represents a significant enhancement of the capabilities of both the GEOS ESM and GEOS-Chem.

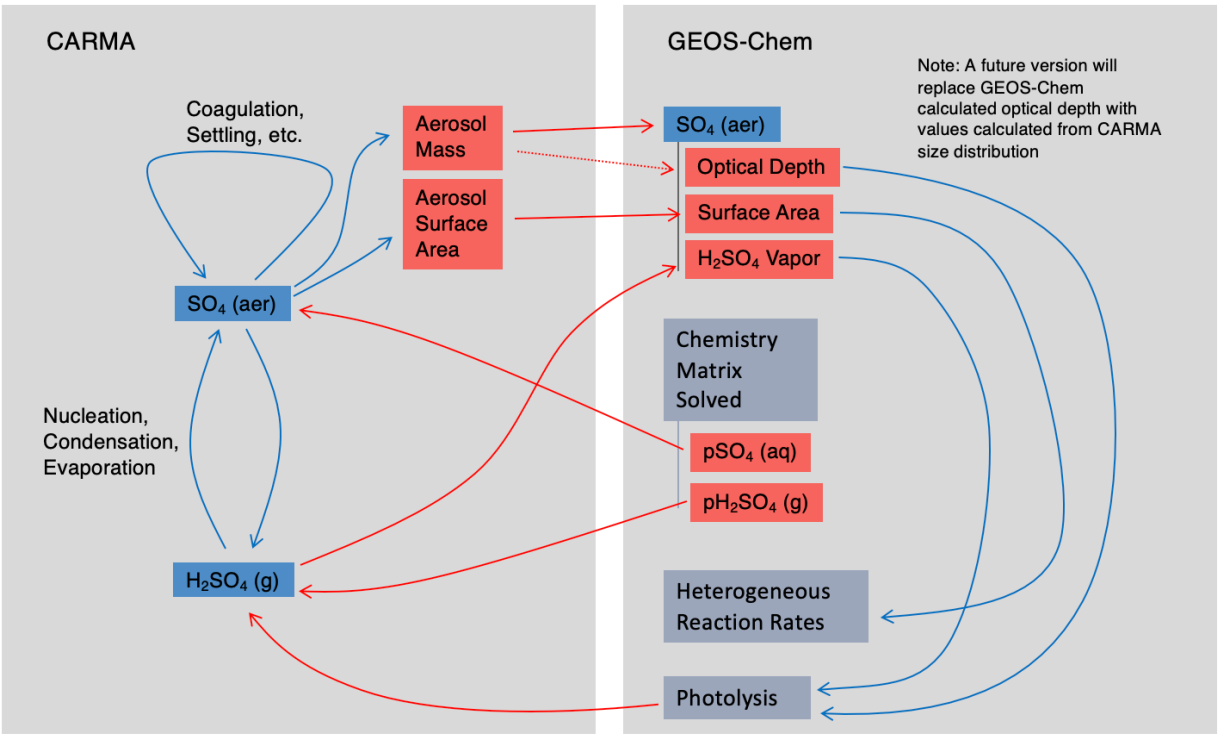

Figure 2.1: A diagram representing the coupling between CARMA and GEOS-Chem. Blue boxes represent tracked species by each model, red boxes represent diagnosed values in each model, and grey boxes represent sub-models or processes. Connections shown with a blue arrow show intra-model connections while red arrows show inter-model connections.

2.3 Initial Conditions and Injection Parameters

The model was spun up at perpetual 1990 conditions of ozone depleting substances, greenhouse gases, and aerosols for 10 model years prior to conducting the experiment. Non-volcanic stratospheric sulfur comes primarily from biogenically generated surface emissions of carbonyl sulfide (OCS) that is relatively inert in the troposphere but oxidizes to SO_2 in the stratosphere and then forms sulfate. Stratospheric sulfate results also from anthropogenic and natural SO_2 sources (and precursors; e.g., DMS) in the troposphere that are transported to the stratosphere (Kremser et al., 2016). Anthropogenic emissions in the model come from the EDGAR HTAP database (Janssens-Maenhout et al., 2015). We have verified both the loading and simulated size distribution of the CARMA-calculated background stratospheric aerosol layer based on these emissions using balloon-borne optical particle counter (OPC) observations. Degassing (non-explosive) volcanoes also provide a source of SO_2 but are not included as a source in this study. A constant surface boundary condition of carbonyl sulfide (OCS) of 500 pptv and a dimethyl sulfide (DMS) emissions climatology, respectively, are prescribed in the model.

We use Pinatubo injection parameters similar to those in Mills et al. (2016). For the primary ensemble, we inject the Pinatubo SO_2 uniformly between 0° and 15°N from 18 to 21 km at 120°E on June 15, 1991. The location of this injection is based on TOMS observations in the days following the eruption (Bluth et al., 1992). We use this distributed injection to account for the unique meteorological situation in the region at the time of the eruption, which caused rapid southward transport.

To test the sensitivity to the injection amount and to account for the uncertainty associated with the Pinatubo injection parameters, we completed a three-member simulation ensemble injecting 10 Tg of SO_2 (5 Tg S) and a separate three-member ensemble injecting 20 Tg of SO_2 (10 Tg S).

Cerro Hudson was a smaller eruption than Pinatubo with less extreme local meteorology, so we use more localized injection parameters. Based on SO_2 mass estimates by Carn et al. (2016) using TOMS, HIRS/2, and SBUV data, we inject 2.6 Tg of SO_2 (1.3 Tg S) from 13 to 18 km directly over the volcano over 24 hours on the day of the eruption, August 15, 1991. Cerro Hudson has been included in both the 10 Tg and 20 Tg ensemble. To evaluate the individual impact of Pinatubo, we also completed a simulation without the Cerro Hudson, using the 20 Tg Pinatubo injection parameters.

We summarize our series of experiments in Table 1.

Experiment	Description
10 Tg ensemble (3 members)	Fully coupled, free running simulations with a Pinatubo injection of 10 Tg SO_2 spread out between 0°-14°N and between 18-21 km at 120°E The Cerro Hudson eruption is also included as a 2.6 Tg injection directly over the volcano (45°S, 72°W).
20 Tg ensemble (3 members)	Same as primary ensemble, with twice as much (20 Tg) SO_2 injected from the Pinatubo eruption.

No Cerro Hudson (3 member)	Same as 20 Tg ensemble, without Cerro Hudson eruption
Background/control (1 member)	2 year simulation at 1991 (without eruptions) conditions after the 10 year spin up (no volcanic SO_2).

Table 1: Experiment names and descriptions.

2.4 Observational Datasets

In order to validate the model, we use various space-based sensors as well as balloon-borne optical particle counter measurements. The main satellite instrument used to observe stratospheric aerosols during the Pinatubo era is the second Stratospheric Aerosol and Gas Experiment (SAGE II) flown on board the Earth Radiation Budget Satellite (ERBS) from 1984 - 2005. SAGE II made solar occultation measurements and provided a long-term space-based record of stratospheric aerosol, and alongside its predecessors and successors we have a record extending from the 1970s to the present. The version of the SAGE II record used in this study is part of the Global Space-based Stratospheric Aerosol Climatology (GloSSAC), which has supplemented the SAGE observations with available air- and ground-based LIDAR as well as other satellite observations (Kovilakam et al., 2020). These supplemental data are especially important in the months following the Pinatubo eruption during which time SAGE II was not able to make measurements because of the extreme optical thickness of the resulting stratospheric aerosol layer (Kovilakam et al., 2020).

In addition to SAGE II, we use an aerosol record of the Pinatubo era from the Advanced Very High-Resolution Radiometer (AVHRR) on the NOAA-11 satellite (Long & Stowe, 1994). This record is based on backscattered sunlight measured at 0.63 μm over oceans and has been corrected to total aerosol optical thickness at wavelength 0.5 μm. A "climatology" of the tropospheric aerosol loading is then subtracted from these data based on 1989 and 1990, two volcanically quiescent years. While this record is not a direct observation of stratospheric aerosol like SAGE II, it is a useful dataset as a single-instrument record with good spatial coverage of the densest parts of the Pinatubo aerosol while the SAGE II/GloSSAC record depends on disparate sources of observations and SAGE II only covers the Earth very slowly.

To validate the model's treatment of gaseous SO_2 in the Pinatubo and Cerro Hudson plumes, we use data from the Total Ozone Mapping Spectrometer (TOMS), the Television Infrared Observation Satellite (TIROS) Optical Vertical Sounder (TOVS) High Resolution Infrared Sounder sensor, and the Microwave Limb Sounder (MLS). TOMS is an ultraviolet sensor that takes measurements at 6 wavelengths while the High-Resolution Infrared Radiation Sounder Version 2 (TOVS/HIRS/2) is an infrared sensor that observes 20 wavelengths. These two satellites are used here, as compiled by Guo et al. (2004), to estimate the total mass of the Pinatubo plume. In order to validate the altitude of the Pinatubo plume we use additional data from MLS from its first few operational days. MLS became

operational on September 19th, 1991 and was immediately used to observe the fading Pinatubo SO_2 plume.

Finally, we use optical particle counter (OPC) observations from the long-term dataset over Laramie, WY (Deshler et al., 2019). These balloon-borne measurements represent a rare in situ observation of stratospheric aerosol. They are useful in validating the output of a sectional aerosol model like CARMA independent of uncertainty added by the optical calculations required to compare with satellite observations. Deshler et al. (2019) report completing 13 balloon flights in 1991 after the eruption of Pinatubo, eight in the months before the plume reached the latitude of Laramie, and five more in the months after.

2.5 Results

GEOS/CARMA was used to simulate the impacts of volcanic aerosols from the 1991 eruptions of Mt. Pinatubo and Cerro Hudson on stratospheric chemistry and aerosols. We first evaluate the model in terms of the available satellite aerosol observations. Because SAGE II was saturated during the period immediately following the eruption, here we focus on the AVHRR record and the SAGE record supplemented by LIDAR observations during June 1991, as described by Thomason et al. (2018). According to AVHRR, the global average stratospheric aerosol optical depth (sAOD) reached a maximum of 0.155 three months after the eruption, in September 1991 (Fig. 2.2). The GEOS/CARMA 10 Tg injection ensemble more closely matches this behavior in the global average. All model results and the SAGE

observations in Fig. 2.2 have been masked to exclude latitudes without AVHRR observations each month (Fig. 2.3e), which explains the sharp changes on the first of August and September at southern midlatitude (right panel). The ensemble using the 10 Tg SO_2 and the ensemble using the 20 Tg SO_2 Pinatubo injection reach a maximum of 0.16 on November 1st and 0.22 on October 3st, respectively. These two ensembles represent edge cases of estimates of the initial Pinatubo SO_2 injection and represent a range of possible Pinatubo-like eruptions. The AVHRR observations of the early Pinatubo plume are within this range. SAGE II observations of the early plume became saturated and were filled in lidar data from aircraft flights (Thomason et al., 2018). After the initial 3-4 months of increasing sAOD, both observations and simulations show declining sAOD as sulfate production slows and aerosols begin to be removed from the stratosphere.

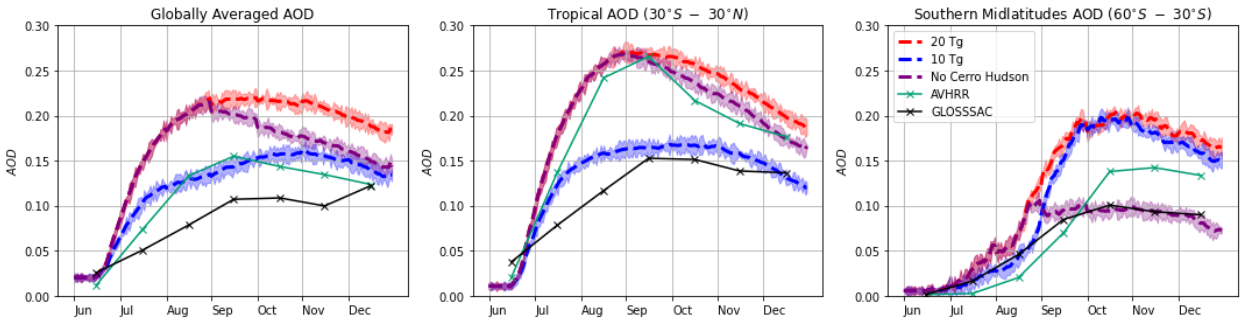

Figure 2.2: Globally averaged stratospheric aerosol optical depth (sAOD) from the GEOS/CARMA 10 Tg (550 nm, blue), 20 Tg (550 nm, red), and no Cerro Hudson ensembles (550 nm, purple), as well as AVHRR (500 nm, grey) and GLoSSAC (525 nm, black). The filled areas around the dashed lines show the ensemble spreads.

The majority of the Pinatubo aerosol remains in the tropical stratosphere throughout 1991. AVHRR observed a maximum tropical (30°S - 30°N) zonally averaged sAOD as high as 0.27 in September, shown in Fig. 2.2. The SAGE II/GloSSAC observations reach a maximum in November at 0.16 zonally averaged tropical sAOD. The 10 Tg ensemble reached a maximum tropical zonally averaged sAOD of 0.16 on October 3rd while the 20 Tg simulation reached a maximum of 0.26 on September 1st. The third panel of Fig. 2.2 shows similarly calculated averages for the Southern Hemisphere midlatitudes (60°S - 30°S) peak at 0.14 in the AVHRR data, 0.10 in the filled SAGE II data.

The comparison between the ensembles with and without the Cerro Hudson eruption indicates that about half of the sAOD in the Southern Hemisphere in 1991 was due to Cerro Hudson aerosols, which increased the sAOD by 0.1 over the simulation without Cerro Hudson. Note that both the SAGE II observations and the model have been masked to match the latitudinal extent of the AVHRR observations each month (see Fig. 2.3e) before these averages were taken.

The meridional spread, magnitude, and lifetime of the tropical Pinatubo aerosol in GEOS/CARMA shows similar features to the observations from AVHRR. Fig. 2.3 shows the zonally averaged sAOD over time in the simulations and observations. The latitudinal extent of the tropical Pinatubo plume in each of the simulations more closely follows the SAGE observations, remaining north of the Equator while AVHRR shows sAOD >0.3 as far South as 15°S. The impact of Cerro Hudson can be seen in both the AVHRR (Fig. 2.3d) and SAGE II (Fig. 2.3e) observations. The

simulation without Cerro Hudson (Fig. 2.3c) shows the contribution of the spread of Pinatubo aerosol south from the tropics, as in Fig. 2.2c.

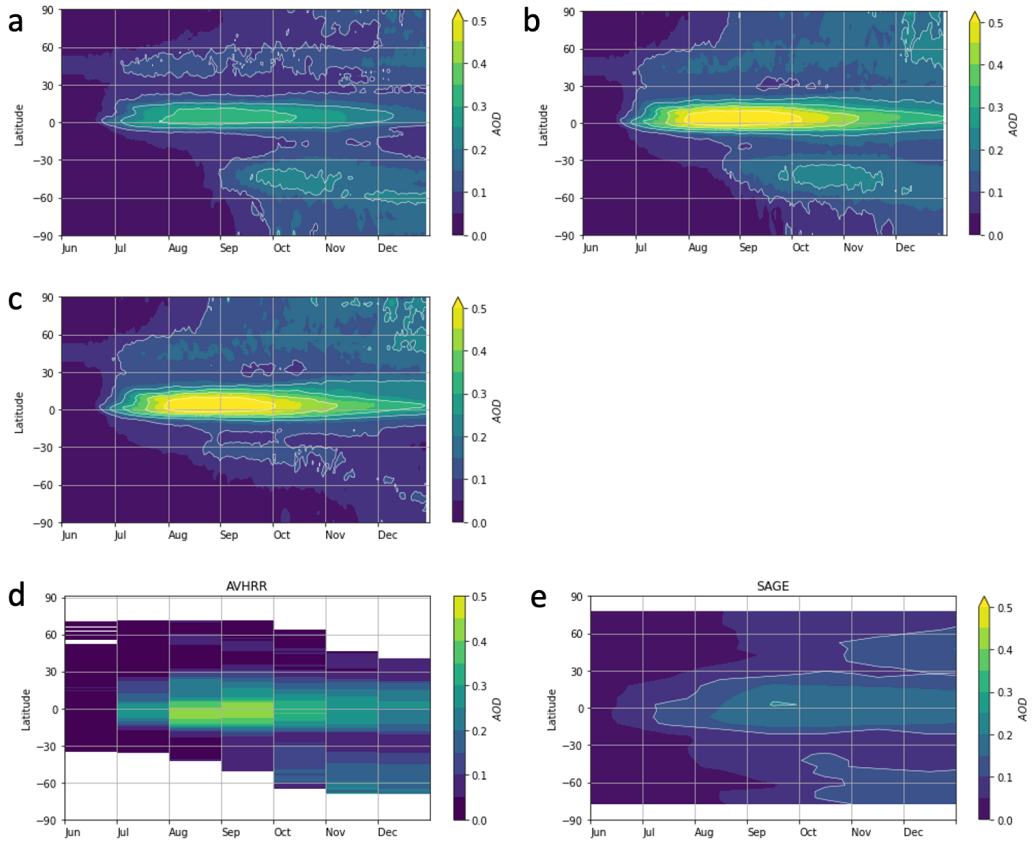

Figure 2.3: Zonal stratospheric aerosol optical depth in the (a) GEOS/CARMA 10 Tg ensemble with 2.6 Tg from Cerro Hudson, (b) GEOS/CARMA 20 Tg ensemble with 2.6 Tg from Cerro Hudson, (c) GEOS/CARMA ensemble without Cerro Hudson, (d) AVHRR, and (e) GLOSSAC.

To evaluate the vertical extent of the Pinatubo plume in the model, Fig. 2.4 shows the comparison of the GLOSSAC observations of tropical (30°S to 30°N) extinction coefficient alongside the model calculated extinction coefficient profile throughout the year. While there are differences in magnitude of the aerosol extinction between GLOSSAC and the modeled values, similar to in Fig. 2.2 and

Fig. 2.3, the altitude of the Pinatubo plume in the model is realistic, especially for the most optically dense part of the plume. The majority of aerosol extinction in the 20 Tg ensemble average is in a layer between 15 and 20km in July; with self-lofting expanding the plume up to 25km by the end of August. A similar pattern can be seen in the observations—while the observed plume is almost entirely below 20km in at the beginning of July, it reaches 28km by the end of August and up to 30km by the end of September. The GLOSSAC observations do show an enhancement of aerosol extinction between 12 and 20km starting in September which is missing from the model. While particles in the simulations are settling, our model is focused on stratospheric sulfates and may underestimate the impact of the Pinatubo aerosol settling into the troposphere because we do not simulate the microphysical interactions of these aerosol with tropospheric species.

To evaluate the simulated quiescent and post-Pinatubo aerosol size distributions, we compare with balloon-borne optical particle counter (OPC) observations taken above Laramie, WY (41°N) in the months following the eruption (Deshler et al., 2019). Deshler et al. (2019) report observing an unperturbed stratospheric aerosol layer until September 18th, 1991. Their next flight, on October 2nd, showed a volcanically perturbed stratospheric aerosol. The observed aerosol count in each OPC channel increased significantly as the Pinatubo aerosol reached Laramie's latitude.

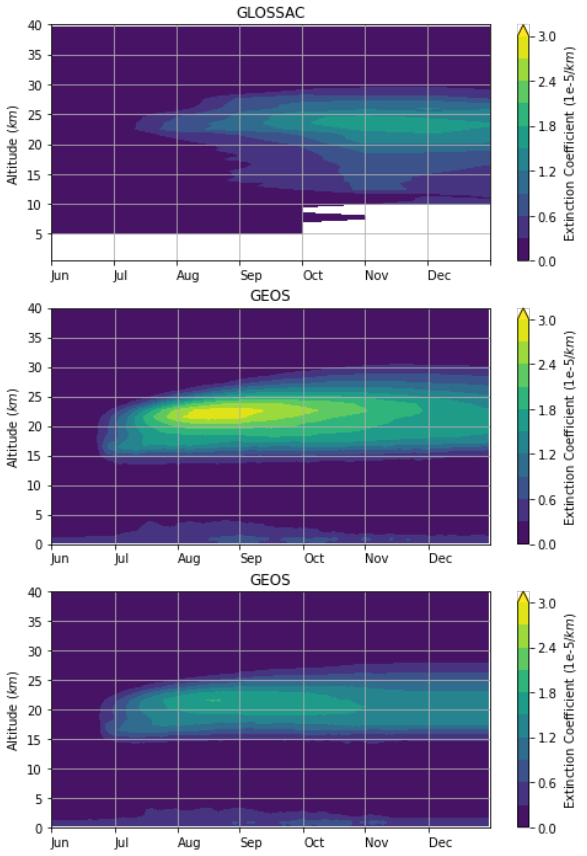

Figure 2.4: Tropical (30°S to 30°N) profile of aerosol extinction coefficient from: (top) the GLOSSAC observational dataset, (middle) the 20 Tg GEOS ensemble mean, and (bottom) the 10 Tg GEOS ensemble mean. In each case, the vertical extent of the plume extends upwards as the plume is self-lofted.

The exact timing of the arrival of the Pinatubo aerosol above Laramie varies between simulations and from the true transport because of the model's free-running meteorology. Fig. 2.5 shows a comparison of the modeled cumulative aerosol size distribution compared with OPC measurements above Laramie, WY. In order to compare with the pre- and post- Pinatubo optical particle counter data, a pre-Pinatubo size distribution is represented by a zonal mean at the latitude of Laramie (41.3°N) of the simulations in July and August and a post-Pinatubo size distribution is represented by a zonal mean of the simulations in November and

December. Both the 10 Tg ensemble and 20 Tg simulation of the pre-Pinatubo stratospheric aerosol are within the spread of OPC observations taken between June 17th and September 18th. The simulations also both show an increase in number of particles by November 15th which generally match the observations taken between October 2nd and December 12th. Both ensembles represent plausible increases in particle density due to the nucleation, growth, and transport of the Pinatubo plume into the Northern mid-latitudes, while the simulated pre-Pinatubo concentrations are in good agreement with the observations of the unperturbed stratosphere.

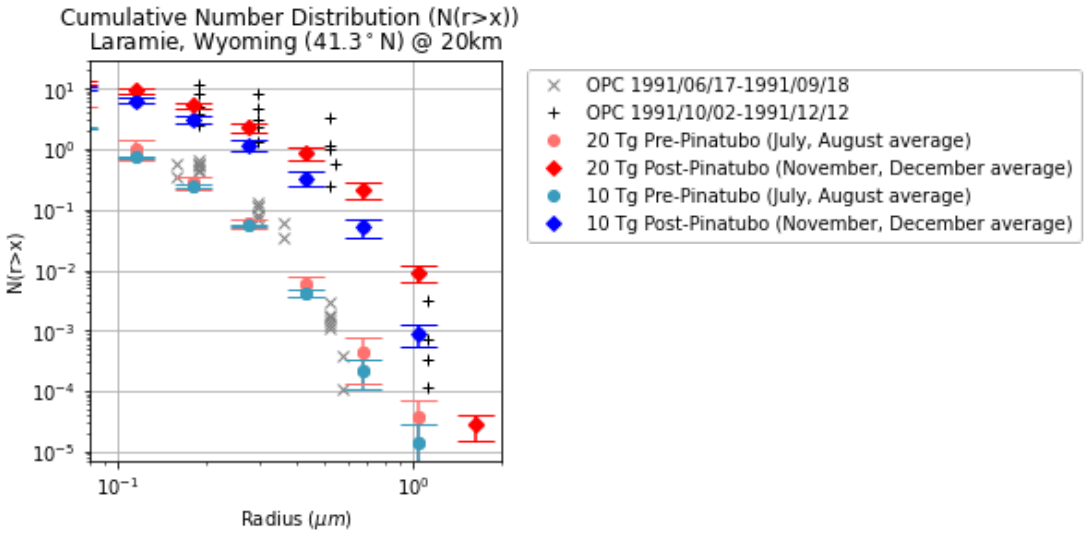

Figure 2.5: Balloon-borne optical particle counter observations from the periods June 17th - September 18th (grey Xs, 8 observations) and October 2nd - December 12th (black +s, 5 observations) from 20 km above Laramie, WY. The number and size of bins in the OPC measurements vary, so each observation is plotted separately. CARMA calculated cumulative aerosol size distributions are also shown. CARMA size distributions are calculated as the zonal average at the latitude of Laramie (41.3°N). A 95% confidence interval is shown for the 10 Tg and 20 Tg ensemble

means. In light blue, the non-volcanic (July and August average) size distribution is shown from the 10 Tg ensemble from August 1st. In light red, the non-volcanic size distribution from the 20 Tg simulation is shown from the same day. A volcanic (November and December average) profile is shown for the 10 Tg ensemble and 20 Tg simulation from November 15th in blue and red. The 20 Tg simulation shows an increase in the number and size of particles more consistent with observations above Laramie, WY.

Fig. 2.6 shows a comparison of the simulations with a zonal average of Microwave Limb Sounder (MLS) observations of the tropical (10°S-10°N) SO_2 on September 21st, 1991 (Read et al., 1993). MLS became operational only on September 19th, 1991, and so was not available to provide insight into the chemistry of the earlier part of the Pinatubo plume. The September 21st, 1991 data provide a boundary condition for the plume chemistry up to that point. The means of the September monthly and zonal average of the 10 Tg and 20 Tg ensemble members are calculated and compared with these observations. The magnitude of the zonally averaged SO_2 in the 20 Tg simulations is comparable to the MLS observations. Both the 10 Tg ensemble and 20 Tg simulation roughly match the height of the plume indicating a realistic rate of self-lofting.

Estimates of the integrated mass of SO_2 in the Pinatubo plume based on TOMS and TOVS HIRS were compiled by Guo et al., 2004 and are shown in Fig. 2.7. These observations, similarly to the observations of sAOD in Fig. 2.2, fit between the 10 Tg (red) and 20 Tg (blue) GEOS/CARMA simulations. Note that TOMS and TOVS differ in their initial estimate of SO_2 mass by more than 1 Tg of sulfur (S), indicating significant uncertainty in the actual mass of the Pinatubo injection.

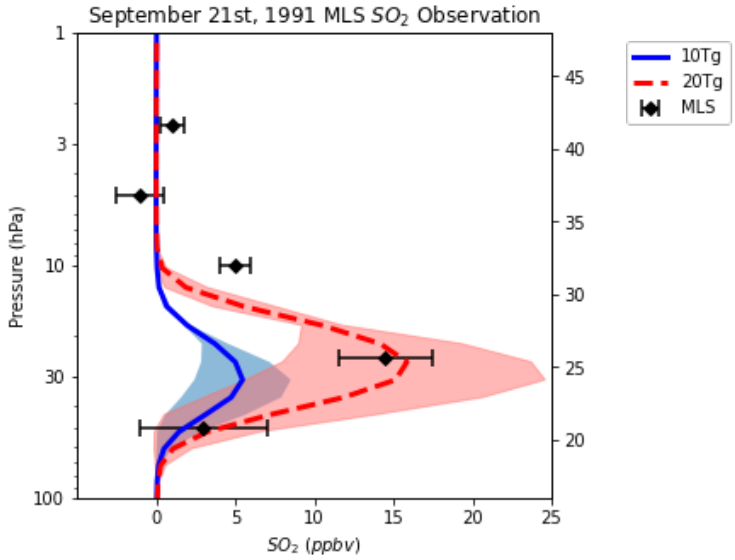

Figure 2.6: Microwave Limb Sounder (MLS) observations of tropical (10°S – 10°N) SO_2 in black (Aquila et al., 2012; Read et al., 1993) and modeled zonal mean tropical profiles from the 10 Tg (blue) and 20 Tg (red) simulations with a 95% confidence interval. The MLS observations are an average of 95 individual SO_2 profiles and the error bars show the retrieval error.

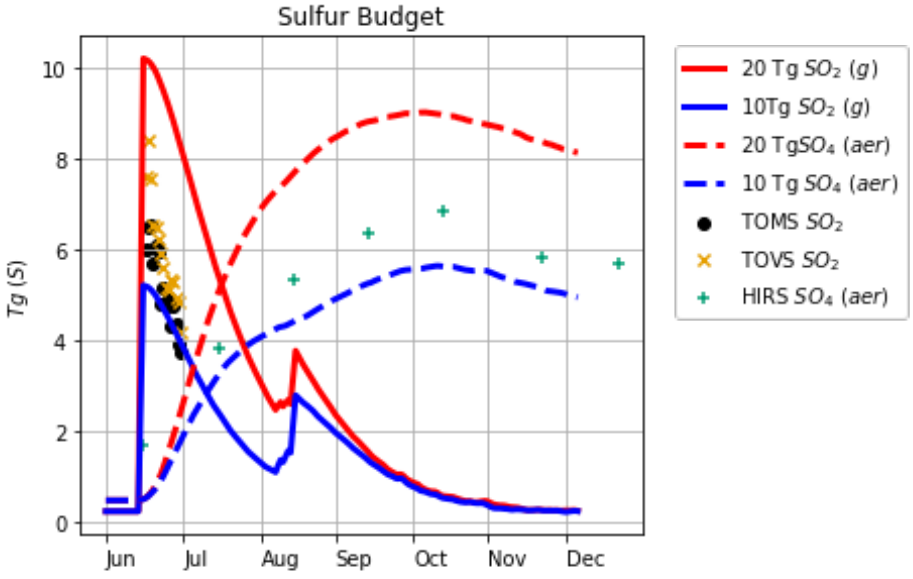

Figure 2.7: Total sulfur (S) mass in SO_2 and sulfate aerosol in GEOS/CARMA. The 10 Tg ensemble average is shown in blue and the 20 Tg ensemble is shown in red. Gaseous SO_2 is shown in the solid lines and aerosol phase sulfate is shown in the dotted lines. TOMS and TOVS observations of total SO_2 mass are shown by mustard and black symbols (Guo et al., 2004). Similarly to aerosol optical depth in Fig. 2.2, the 10 Tg and 20 Tg case bracket the observed Pinatubo plume.

Finally, we estimate the impact of OH depletion on the conversion of SO_2 to sulfate in the Pinatubo plume. Observations of the early Pinatubo plume were sparse, but the SO_2 lifetime in the plume was characterized from estimates of the initial SO_2 mass injected and tracking of the plume in the subsequent weeks. The e-folding time of SO_2 within the Pinatubo plume, i.e., the time it takes for the mass of SO_2 to decrease to 1/e of its initial value, has thus been observationally constrained to be between 23 and 35 days (Guo et al., 2004; Bluth et al., 1991). This approach to measuring the oxidation rate of SO_2 in the plume assumes a near-constant concentration of OH, resulting in a constant e-folding time, no matter the time horizon it is calculated for. When calculated consistently in our model this "average" e-folding time, or the time for the Pinatubo SO_2 to decrease by a factor of 1/e is 34 days in the 10 Tg ensemble and 36 days in the 20 Tg ensemble, consistent with earlier GEOS simulations that used prescribed oxidant fields, as in Aquila et al. (2012). Importantly, though, those earlier "uncoupled" simulations were found to have too rapid of SO2 to sulfate immediately after the eruption.

The e-folding time estimates noted above are effective over a long period in the run, but they do not illustrate the rate of change of the SO_2 consumption in the plume due to depletion of the oxidants. The coupled aerosol-chemistry model used here allows us to assess the SO_2 lifetime at a finer timescale than previous versions

of the model. In order to quantify the dynamic lifetime of SO_2 in the oxidant poor plume, we calculate the instantaneous e-folding time of SO_2 in our model, as in Mills et al. (2016). Instantaneous e-folding time is defined as the time it would take to reach 1/e of the current mass at the current rate of oxidation, calculated using daily averages in the model. Fig. 2.8 shows the instantaneous e-folding time for the 10 Tg ensemble and 20 Tg ensemble. In the 10 Tg ensemble, a maximum e-folding time of 169 days is reached the day after the eruption, before approaching an asymptote of 31.7 days by August 1st. The 20 Tg ensemble showed a more extreme OH response, reaching a maximum e-folding time of 202 days the day after the eruption before approaching an asymptote of 30.2 days by August 1st.

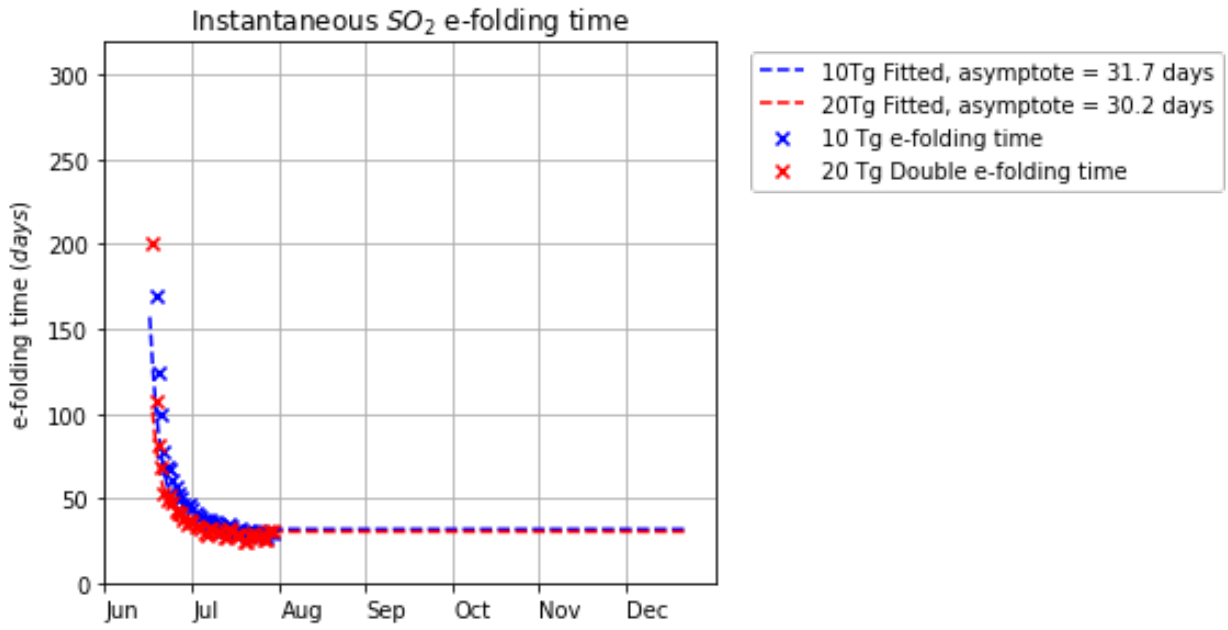

Figure 2.8: Instantaneous SO_2 e-folding time from the GEOS/CARMA 10 Tg ensemble (blue) and 20 Tg ensemble (red). The e-folding time peaks at 241 days the day after the eruption in the 10 Tg case while it peaks at 292 days in the 20 Tg case.

Both cases have been fitted to an exponential decay function, the 10 Tg case asymptotes to 31.7 days while the 20 Tg case asymptotes to 30.2 days.

2.6 Conclusions and Discussion

We have used remote sensing data (SAGE II, AVHRR, TOMS, MLS, and TOVS) alongside in situ optical particle counter observations to evaluate a new capability of the GEOS Earth system model to perform coupled aerosol, chemistry, radiation, and dynamics simulations. We focus here on the 1991 volcanic eruption of Mt. Pinatubo because it is much studied in the literature and gives us a benchmark to compare against, both in terms of observations and previous models. Our model includes the detailed stratospheric and tropospheric chemistry of the GEOS-Chem mechanism coupled to the CARMA sectional aerosol microphysics model. This approach allows us for the first time to simulate with GEOS the detailed microphysical response of volcanic sulfates and their perturbation to the quiescent stratospheric background aerosol in a framework that allows for realistic depletion of oxidants in the dense volcanic plume.

The GEOS/GEOS-Chem/CARMA model simulates an eruption based on the 1991 eruption of Mt. Pinatubo. It simulates a perturbation to the background aerosol with similar magnitude and temporal evolution to what was observed in 1991. This work highlights this model's sulfur chemistry mechanism, which, as part of the broader GEOS-Chem mechanism, interactively simulates the impact of a volcanic SO_2 plume on broader stratospheric chemistry. These simulations also show the model's skill in evolving a realistic aerosol size distribution following a

volcanic eruption. The mass of injected SO_2 associated with the June 15, 1991, eruption of Pinatubo remains uncertain due to the lack of early observations and the coincident Typhoon Yunya. This work demonstrates that the global stratospheric impacts of Pinatubo can be modeled by an injection of SO_2 based on TOMS observations in the days following the eruption. The GEOS/GEOS-Chem/CARMA model indicates that an injection of 10 Tg of SO_2 is adequate to explain space-based AOD observations but that early MLS measurements of SO_2 and in situ OPC observations may indicate that an injection of 20 Tg results in the model more closely matching observations in the final months of 1991.

We additionally use the model to characterize the impact of the Pinatubo and Cerro Hudson eruptions on Southern Hemisphere sAOD in the months following Pinatubo. According to our model, about 50% of the AOD in the Southern Hemisphere in the six months following Pinatubo can be attributed to Cerro Hudson. As shown in Fig. 2.2c, our ensemble without the Cerro Hudson eruption produces an increase in Southern Hemisphere sAOD as Pinatubo aerosol are transported at high altitudes into the Southern Hemisphere midlatitudes, consistent with the findings of Aquila et al. (2013). In comparison, the simulations which included both eruptions show an additional 0.1 sAOD from the Cerro Hudson eruption. Our simulations indicate that including Cerro Hudson is important in future modeling studies of the Pinatubo eruption.

These simulations also support the hypothesis that major OH depletion happened in the early Pinatubo plume. A decrease in the decay rate of SO_2 of

similar magnitude to Mills et al. (2017) is calculated by the GEOS-Chem chemistry mechanism, represented by an increase in the e-folding time from a background value of 30 to 31 days to more than 200 days. While observations of SO_2 from the weeks following the eruption are too coarse to see this effect, our simulations indicate that this effect is significant in eruptions of similar magnitude as the 1991 eruption of Mt. Pinatubo. Further work is necessary to quantify the magnitude of this effect in smaller eruptions in the satellite record. Zhu et al. (2020) also reported in a simulation of Kelud that SO_2 may undergo heterogeneous reactions on ash. Such reactions are not included in our simulations, but they might have resulted in a loss of SO_2 more rapid than in our simulations.

Further analysis of the 1991 eruption of Mt. Pinatubo is needed to fully understand the processes that led to its ultimate impacts on the Earth system. Specifically, our model, because of its resolution and global scope, is not equipped to resolve the meteorological situation on the day of the eruption. For this reason, we have not attempted to find the "true" mass of injected SO_2 from the eruption and instead have mapped the model's sensitivity to a roughly Pinatubo-sized eruption. A regional, finer resolution model would be better equipped to estimate the initial mass of SO_2 and other eruptive gasses and aerosols, as in Stenchikov et al. (2021). Even within the scope of global modeling, a better understanding of the interaction of SO_2, sulfate aerosols, and ash aerosols in volcanic plumes could constrain the appropriate injection parameters and impacts of the Pinatubo eruption.

The simulations presented here build upon previous work simulating Pinatubo in global models. Previous work surrounding Pinatubo, including work sharing model components with the simulations presented here, provides useful context in interpreting the significance of these simulations. Early, two dimensional global models simulating Pinatubo-like eruptions suggested that OH depletion in the volcanic plume was negligible compared to the rate at which it was replaced and that it would require an eruption ten times larger to see a change in the SO_2 removal rate (Bekki, 1995). The localized effect of OH depletion within the Pinatubo plume, however, is resolved in more contemporary three dimensional models, like the one presented here and the one used in Mills et al., 2017.

Fig. 2.9 shows the simulated stratospheric aerosol optical depth from three previous Pinatubo studies (Aquila et al., 2012; English et al., 2012; and Niemeier et al., 2009), comparable to Fig. 2.3, none of which include the August eruption of Cerro Hudson. The tropical reservoir of Pinatubo aerosols reaches a peak optical thickness of between 0.45 and 0.5, similar to the 20 Tg ensemble in the GEOS/GC/CARMA model. In each of these cases, Southern Hemisphere (60°S-30°S) sAOD stays below 0.1, similar to our own simulations that excluded Cerro Hudson, but these results clearly underestimate the values observed by the satellite-based sensors. These earlier studies are thus consistent with our findings that about half of the optical depth observed in the Southern midlatitudes during 1991 were a result of the Cerro Hudson eruption. While injection altitude, local meteorology, and plume self-lofting mentioned in these studies are important effects in getting

Pinatubo aerosol to the Southern Hemisphere, the impact of Cerro Hudson is equally as important.

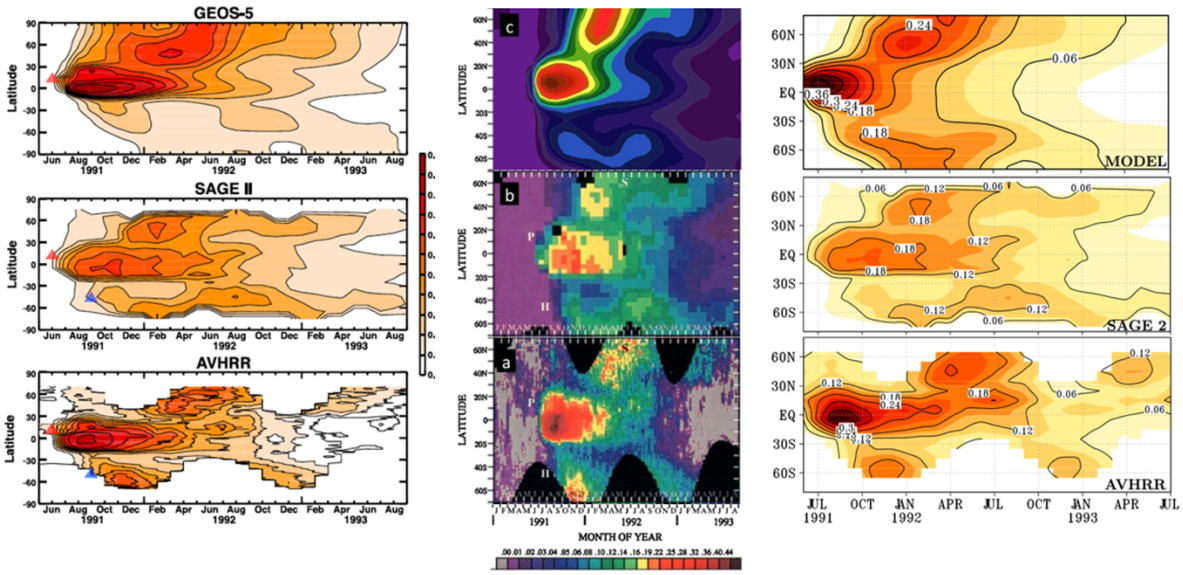

Figure 2.9: Stratospheric aerosol optical thickness at 550 nm from (left) Aquila et al., 2012, (center) English et al., 2012, and (right) Niemeier et al., 2009. Each column includes model-calculated optical depth alongside the observed sAOD from SAGE II and AVHRR. These results are comparable to Fig. 2.3.

The model presented in this work could be used to characterize the dynamic stratospheric aerosol in the more recent volcanic record, and could inform observations of the stratosphere moving forward. The stratospheric aerosols satellite record after Pinatubo includes a volcanically quiescent period until 2000, followed by a decade characterized by many relatively small tropical eruptions, which have been shown to have caused the majority of sAOD variability (Neely et al., 2013; Carn et al., 2016). The model developed for this study is well equipped to characterize the stratospheric aerosol of this period. Volcanic ash aerosols, though generally short-lived, have been shown to alter the long-term impacts of volcanic

eruptions via heterogeneous oxidation of SO_2 as well as acting as a sink for sulfate mass as they settle out of the stratosphere. Future model developments are planned to include these effects. Recent work has also shown the impact of aerosols from pyrocumulonimbus events on the stratosphere can be of similar magnitude to volcanic eruptions. We plan to incorporate carbonaceous aerosols into the model to study these events and their interactions with the background stratosphere and volcanic eruptions.

CHAPTER III

SIMULATING THE VOLCANIC SULFATE AEROSOLS FROM THE 1991 ERUPTIONS OF PINATUBO AND CERRO HUDSON AND THEIR IMPACT ON THE 1991 OZONE HOLE

3.1 Introduction

Two months after the 1991 eruption of Mount Pinatubo (15°N, 120°E), the largest stratospheric volcanic injection in the satellite record, the Chilean stratovolcano Cerro Hudson (45°S, 72°W) erupted. While the sulfur dioxide (SO_2) emissions to the stratosphere of the Cerro Hudson eruptions occurring between August 8th and 15th were dwarfed by the June 15th Pinatubo eruption, it remains as the fifth largest eruption by SO_2 emissions observed by satellites (Carn et al., 2016). The initial Cerro Hudson injection is estimated to have put 1.7-2.9 Tg of SO_2 and a similar amount of ash between 16-18km (Bluth et al., 1992; Constantine et al., 2000; Miles et al., 2017). The ash and SO_2 plumes quickly separated and about 90% of the ash fell out in the first few days following the eruption, mostly settling across South America (Constantine et al., 2000).

The SO_2 plume, observed by the Total Ozone Mapping Spectrometer (TOMS) (Bluth et al., 1992) and the High Resolution Infra-Red Radiation Sounder/2 (HIRS/2) (Miles et al., 2017) instruments, remained in the lower stratosphere between 50°S and 70°S as it circled the Earth, returning to the longitude of the volcano on August 21st, 7 days after the eruption (Doiron et al., 1991; Schoelberl et al., 1993). The Microwave Limb Sounder (MLS), also capable of retrieving SO_2,

came online in September, 1991, and while it was able to make useful observations of the tropical Cerro Hudson plume, produced noisy results at the altitude and latitude of the Cerro Hudson plume (Miles et al., 2017).

On September 10th and daily after September 20 the Cerro Hudson plume was observed by lidar and balloon-borne optical particle counters within the Antarctic polar vortex over McMurdo (Deshler et al., 1992; Hofmann et al., 1992). The low altitude of the volcanic aerosol layer, between 9 and 13 km, combined with the presence of newly nucleated aerosols at very high concentrations indicated that this aerosol was from the Cerro Hudson plume. Observations of the Pinatubo aerosol, on the other hand, showed little aerosol below 17km. Deshler et al. and Hofmann et al. also showed that the normally invariable low-altitude ozone measurements at 12 km showed anomalously low ozone concentrations, with 50% depletion, beginning in late September, 1991 when compared with other years with similar amounts of Antarctic ozone loss. The rate of ozone loss was 4-8 ppb day^{-1} over 30 days. Satellite observations of SO_2 for 19 days after the Cerro Hudson eruption did not show the SO_2 entering the vortex before the beginning of September (Krueger et al., 1992). Trajectory model results suggested that the volcanic plume remained outside of the vortex during the season of ozone depletion (Krueger et al., 1992), but these models are inconsistent with the direct observations of volcanic aerosols in the vortex below 13 km during mid- to late September when significant ozone loss was found and trajectory models are only useful for about 10 days (Deshler et al., 1992; Hofmann et al., 1992).

Studies of more contemporary volcanic eruptions that occurred in the Southern midlatitudes during the Austral Winter show that even moderately sized eruptions at these latitudes can impact the Springtime ozone loss, especially as the polar vortex begins to break down in September (Solomon et al., 2016; Zhu et al., 2018). In the case of the April 2015 Calbuco eruptions (Zhu et al., 2018), observations and models show that transport of volcanic aerosols into the vortex occurred as early as May, allowing them to alter polar stratospheric clouds and ultimately the chemistry of springtime ozone depletion. Cerro Hudson provides an interesting case in that the eruption was similar in latitude and magnitude to Calbuco but occurred four months later in the year. Despite this later eruption date, Deshler et al., 1992 have shown that Cerro Hudson aerosol appeared at high Southern latitudes and potentially impacted ozone observations in September and October.

We have simulated the 1991 eruption of Cerro Hudson using the Goddard Earth Observing System (GEOS) global model coupled with a sectional aerosol microphysics module, the Community Aerosol and Radiation Model for Atmospheres (CARMA), and the tropospheric and stratospheric chemistry module GEOS-Chem (GC). Here we show that (i) the GEOS/CARMA/GC model can reasonably reproduce both the satellite and balloon-born in-situ observations of the Cerro Hudson plume, that (ii) Cerro Hudson aerosol did reach high Southern latitudes and impacted ozone below 20 km while remaining outside the vortex above 20 km, and that (iii) while it is unlikely that the volcanic aerosols directly altered

the ozone chemistry above 20 km in 1991, the dynamical response to these aerosols resulted in a more persistent vortex and lower ozone values above 20km.

3.2 Methods and Model Description

GEOS is an Earth system model based on the architecture of the Earth System Modeling Framework (ESMF) (Hill et al., 2004; Molod et al., 2015). In this study, we use the atmospheric general circulation model (AGCM) configuration in its "free-running" mode; the model calculates its own meteorology without any data assimilation and with imposed sea surface temperatures based on observations. The GEOS system has been shown to perform well in stratospheric chemistry and transport processes (SPARC CCMVal, 2010; Strahan et al., 2011; Douglass et al., 2012). We run GEOS at a ~100 km horizontal resolution on a cubed-sphere grid with 72 hybrid-sigma vertical levels extending from the surface to ~80 km. While the GEOS AGCM can be coupled to various aerosol modules, here we are using the sectional aerosol microphysics from the Community Aerosol and Radiation Model for Atmospheres (CARMA, Toon et al., 1988; Bardeen et al., 2008). CARMA was previously coupled to GEOS for dust and sea salt (Colarco et al. 2014). Here we have coupled CARMA to the GEOS-Chem tropospheric and stratospheric chemistry mechanism (Bey et al., 2001; acmg.seas.harvared.edu/geos/), and both CARMA and GEOS-Chem are radiatively interactive within the model. For a complete description of GEOS-Chem, CARMA, and the coupling of the GEOS/GC/CARMA model, see Case et al. (2022 Submitted).

A total of nine simulations are used as part of this study, separated into three ensembles. First, a three-member background ensemble represents the second half of 1991 without the Pinatubo or Cerro Hudson eruptions. A second three-member ensemble includes only the Pinatubo eruption over the same period and a final ensemble includes both the Pinatubo eruption as well as the Cerro Hudson eruption. Ensemble members are perturbed at the beginning of 1991 to develop varying meteorological and dynamical situations.

Cerro Hudson is represented in the model by an injection of 2.7 Tg of SO_2 between 16 and 18km in the grid column above the volcano, spread out over 24 hours on the day of the largest eruption (August 15). We use Pinatubo injection parameters similar to those in Mills et al. (2017). For Pinatubo, we inject 10 Tg SO_2 over 25 hours on June 15, 1991 uniformly mixed from 18 to 21 km altitude between 0° and 15°N over a 1 degree wide longitude region centered at 120°E. The location of this injection is based on TOMS observations in the days following the eruption (Bluth et al., 1992). We use this distributed injection to account for the unique meteorological situation in the region at the time of the eruption, in which a typhoon caused rapid southward transport.

3.3 Results and Discussion

The GEOS/GC/CARMA model shows similar transport to that observed by satellite around the Southern midlatitudes in the first week following the eruption of Cerro Hudson on August 15th (Fig. 3.1). HIRS/2 and TOMS observations for each

day alongside the modeled SO_2 column concentration are shown in Fig. 3.1. The modeled SO_2 plume shows a similar magnitude to the HIRS and TOMS observations. An average peak value of 109 DU in the model ensemble is slightly lower than the 130+ DU peak observations. By the time the plume returned to the longitude of the volcano, the modeled plume has a peak SO_2 column of 16 DU while observations as high as 50 DU were observed by both instruments. The horizontal extent of the plume is wider in the modeled field, indicating that the lower peak values are in part due to the coarse resolution of the model.

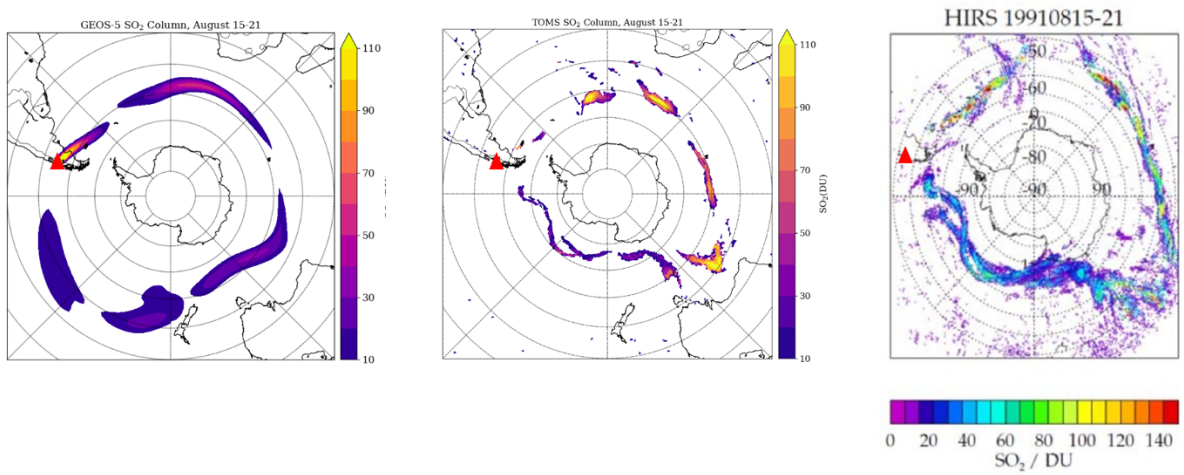

Figure 3.1: Seven-day composite of one instance of model calculated (left) and satellite retrieved (middle, right) SO_2 column concentrations as the Cerro Hudson plume transits the Southern midlatitudes. The August 15 observation in each panel is shown above Cerro Hudson and observations from the six following days are shown clockwise around Antarctica.

The model-calculated zonal mean aerosol size distribution at the latitude of McMurdo Bay, Antarctica (78°S), shows an enhancement in the ensemble including Cerro Hudson when compared to the ensemble not including Cerro Hudson by a

factor of about 3 for each size range. This magnitude of enhancement is consistent with an anomalous aerosol layer observed by Deshler et al., 1992 above McMurdo Bay on September 27th relative to earlier balloon flights. The observed size distribution shows more particles than the model, particularly below 1μm radius, which is partly due to the zonal mean taken in the model to capture the aerosol plume across the separate ensemble members, while the data are from one location.

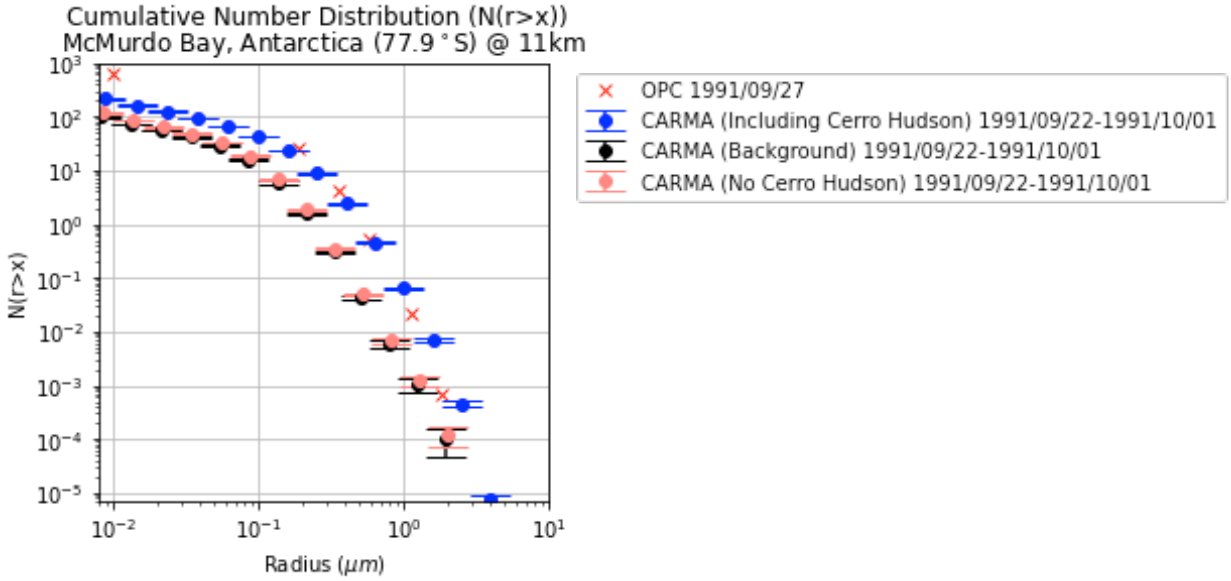

Figure 3.2: Balloon-borne OPC observations above McMurdo Bay on September 27th (red Xs), compared with model-calculated zonal-mean cumulative aerosol size distributions at the latitude of McMurdo for the ensemble including Cerro Hudson (blue dots with error bars) and the ensemble excluding Cerro Hudson but with Pinatubo (red dots with error bars). The black dots are from the no volcanic injections case which varies little from the ensemble excluding Cerro Hudson. The error bars represent the 95% confidence interval across each ensemble.

The Global Space-based Stratospheric Aerosol Climatology (GloSSAC), a climatology of stratospheric aerosols primarily drawn from the Stratospheric Aerosol and Gas Experiment instruments (SAGE), shows a distinct layer of high

extinction in September 1991 below 15 km consistent with the altitude and latitude of the Cerro Hudson volcanic plume as well as a layer above 20 km consistent with Pinatubo (Kovilakam et al., 2020). While the GEOS/GC/CARMA ensembles show more extinction in the lower stratosphere below 20 km between 30°S and 50°S than was observed, there is a clear enhancement of the lower-stratospheric aerosol layer poleward of 50°S consistent with the observed high extinction in the GLOSSAC climatology.

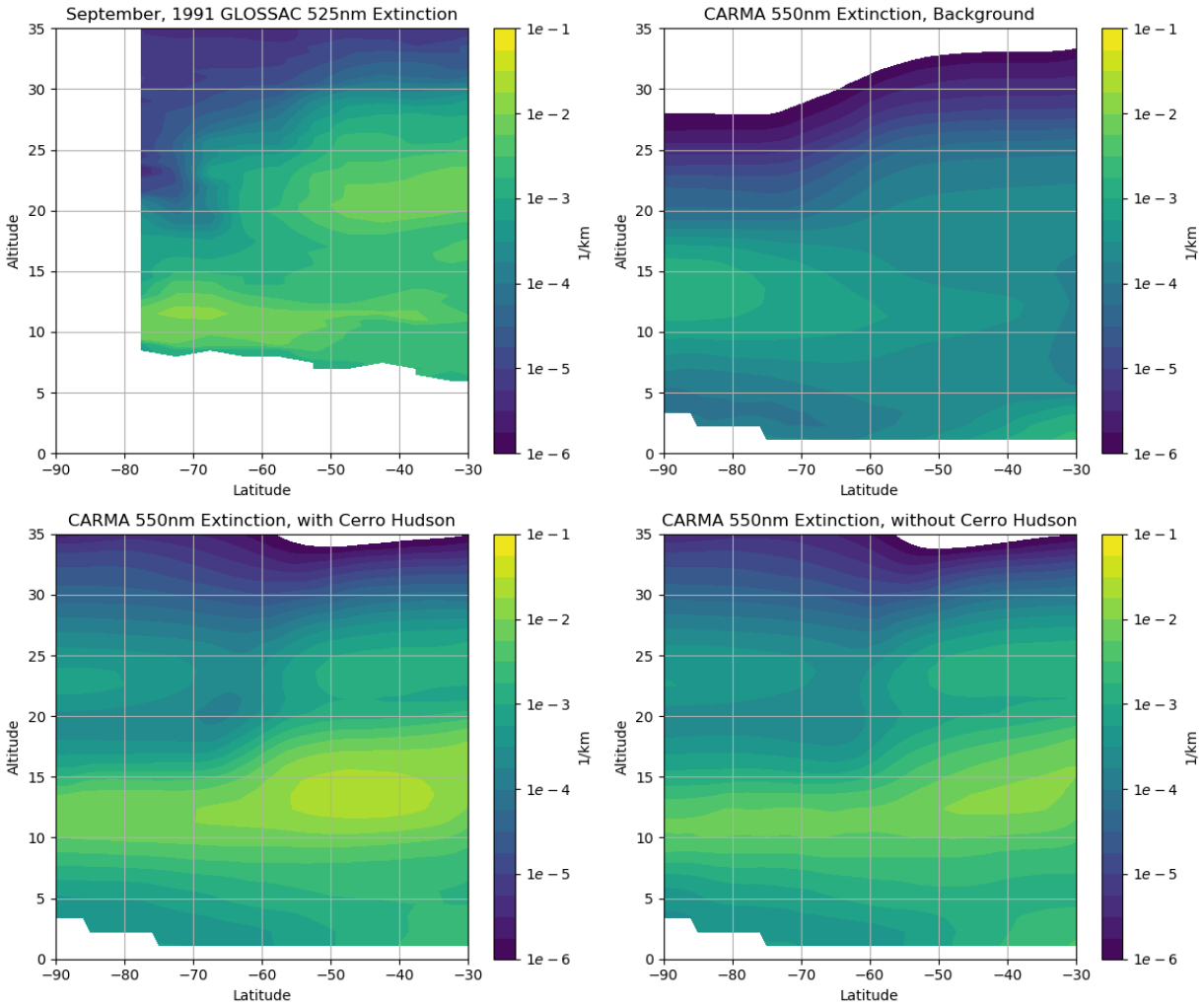

Figure 3.3: Southern Hemisphere zonal mean aerosol extinction in September, 1991 in the GLOSSAC observational climatology (top left), the background ensemble (top right), the ensemble including Cerro Hudson (bottom left) the ensemble excluding Cerro Hudson but including Pinatubo (bottom right).

The portion of the Pinatubo plume that has reached the Southern Hemisphere by September can be seen in both the observations and the modeled extinction. The enhanced extinction between 30°S and 50°S above 20 km shows high altitude transport of Pinatubo aerosols and there is some evidence of lower-altitude Pinatubo aerosol along the tropopause, enhancing the existing lower stratospheric aerosol layer. Both of these features are shown in the modeled extinction fields and have been noted in previous modeling of Pinatubo in GEOS (Aquila et al., 2012). Note that the Pinatubo aerosol in both the observations and the model ensembles remain outside the edge of the vortex above 20 km. The extinction from the Cerro Hudson eruption between 10 km and 15 km is consistent with the balloon observations from Deshler et al.

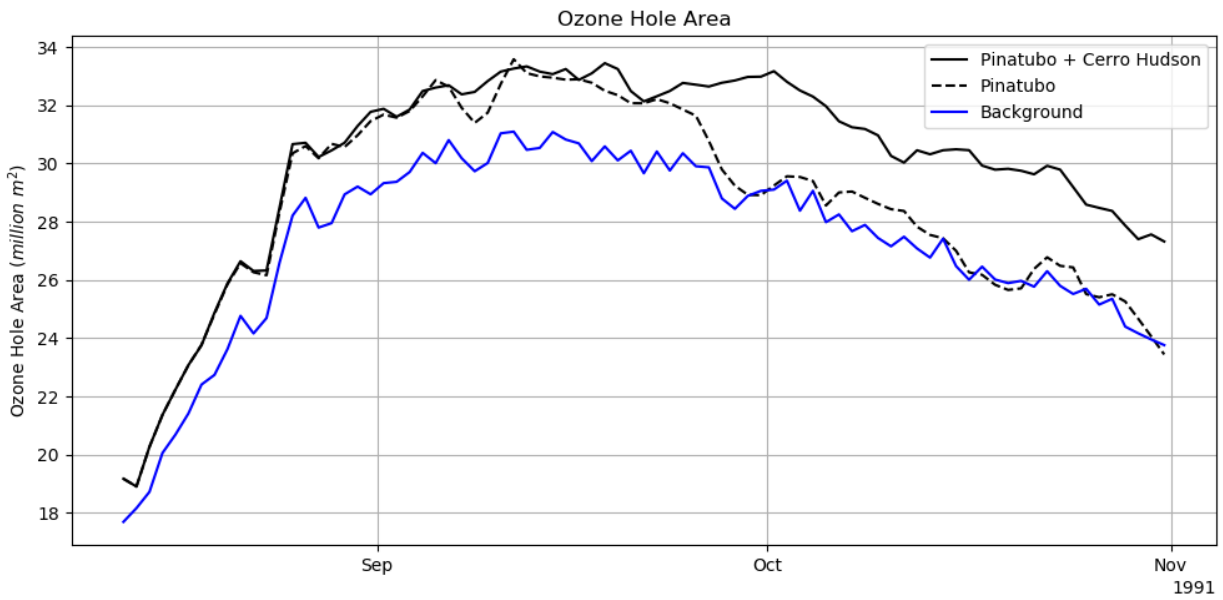

Figure 3.4: Ozone hole area in the GEOS/GC/CARMA model for the ensemble including Cerro Hudson (solid) and the ensemble excluding Cerro Hudson (dashed). In blue, the background model ozone hole area is shown, excluding both eruptions. Note that the model has a low bias in ozone, resulting in high estimates of ozone hole area for 1991.

Model-calculated ozone hole area, defined as the area inside the 220 DU contour, is significantly impacted when the Cerro Hudson eruption is included. Starting in late September, the ensemble including Cerro Hudson has a 5-10% larger ozone hole area continuing throughout October until the vortex breaks down. It should be noted that the model-calculated ozone hole area is larger than observed 1991 values resulting from a low bias in polar ozone in the model. Both ensembles have a similar peak ozone hole area in mid-September but the recovery of ozone values in the ensemble including Cerro Hudson is slowed, lagging the ensemble without Cerro Hudson values by an average of 13 days throughout October. The extra ozone hole area shown in Fig. 3.4 is primarily driven by lower ozone values in

the “collar region”, defined here as the longitudinal ring around the ozone hole between 55°S and 65°S. The model shows 20-40% lower ozone in the collar region in October in the ensemble including Cerro Hudson than in the ensemble without Cerro Hudson from 15 km to 25 km as shown in Fig. 3.5.

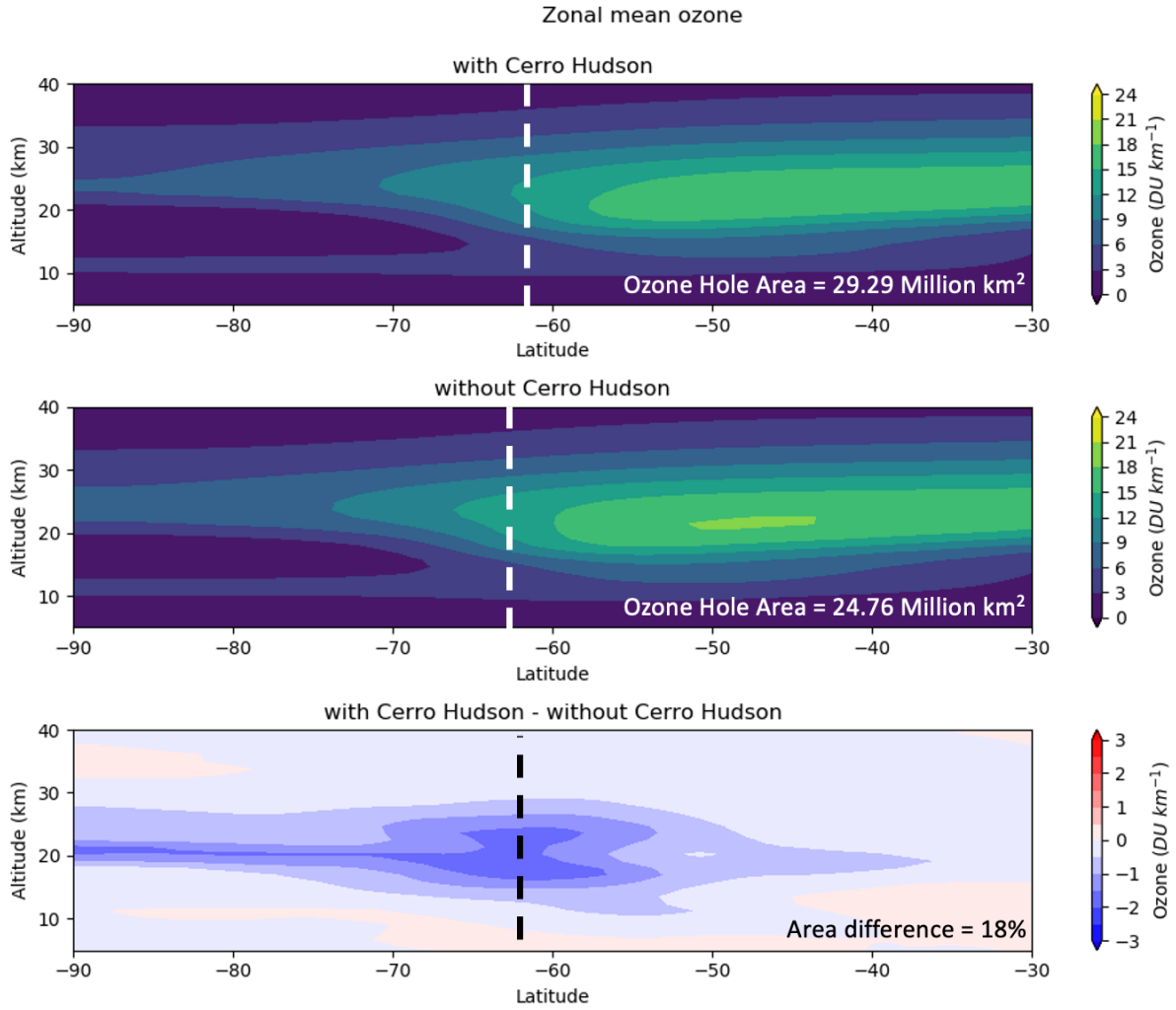

Figure 3.5: October, 1991 zonal mean ozone concentrations in the GEOS/GC/CARMA modeled Southern Hemisphere. Shown are the ozone field and average ozone hole area for the ensemble including Cerro Hudson (top), the ensemble excluding Cerro Hudson (middle), and the difference (bottom). The dotted line on each panel indicates the vortex edge.

The development of the low-ozone collar region in the ensemble including Cerro Hudson is coincident with the start of lower temperatures and lower aerosol surface area when compared with the ensemble not including Cerro Hudson. Fig. 3.6 shows the collar region average ozone concentration, temperature, and aerosol surface area for each ensemble alongside MERRA 2 temperatures for the same time period for two different altitude ranges (20-25 km, 10-20 km). The ensemble average for the background (no volcanic eruptions) ensemble has been subtracted from each of these timeseries, including the MERRA 2 data. Similar to Fig. 3.4, the ensembles meaningfully diverge starting in late September and are significantly different throughout October. While there is a small amount of volcanic aerosol surface area in the region prior to this divergence driven by Pinatubo, once the ensembles diverge, there is less aerosol surface area between 20 and 25 km in the ensemble including Cerro Hudson, despite a higher volcanic aerosol loading in the Southern hemisphere in that ensemble.

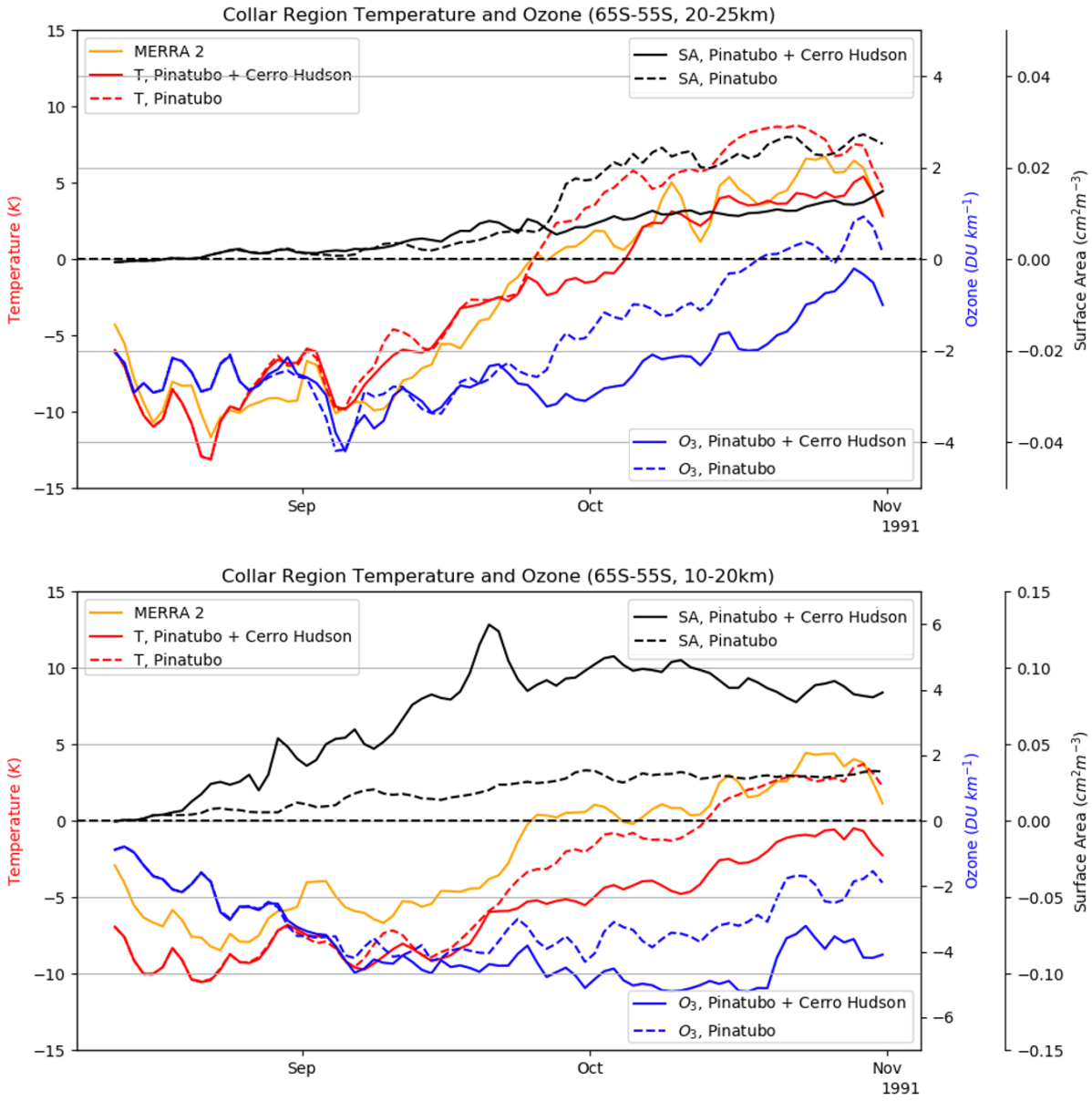

Figure 3.6: (Top) Collar region (55°S to 65°S, 20 to 25 km) temperature (red), ozone concentration (blue), and aerosol surface area concentration (black) anomalies from the background in the ensemble including Cerro Hudson (solid lines) and the ensemble excluding Cerro Hudson (dashed lines). Values near zero indicate that the ensembles are similar to the background ensemble (without Pinatubo or Cerro Hudson); negative anomalies indicate colder temperatures, lower ozone concentrations, and lower surface area concentrations compared with the background simulations. The MERRA-2 temperature for this region is also included

(orange). (Bottom) The same parameters as above, but in the collar region from 10 km to 20 km.

Fig. 3.6 indicates that the difference in ozone concentrations and ultimately ozone hole area, was driven by a combination of a change in the ozone chemistry below 20 km and a dynamical difference above 20 km. Below 20km, additional aerosol surface area from Cerro Hudson is collocated with lower ozone values in the ensemble including Cerro Hudson. By comparison, the coincident lower aerosol surface area and lower ozone above 20 km indicate a dynamical difference in the two ensembles leads to this region's ozone loss. Newman et al., 2004 show that ozone hole size is sensitive to temperatures near the edge of the vortex, which are driven by tropospheric wave forcing to the stratosphere. Fig. 3.7 shows the eddy heat flux, the product of the temperature and meridional wind component anomalies from the zonal mean between 20 km and 25 km. Eddy heat flux is proportional to planetary wave energy being advected vertically into the stratosphere (Edmon et al., 1980) and has been shown to drive temperature and ozone concentrations near the edge of the vortex by controlling the vertical transport of high temperatures and ozone into the polar lower stratosphere (Newman et al., 2001; Newman et al., 2004). Negative values from September 13th through September 19th (3-5 days before the ensembles diverge in the collar region (Fig. 3.6)) indicate a wave event in the ensemble without Cerro Hudson across all members. In the Southern Hemisphere, a negative eddy heat flux means increased vertical transport of high temperatures and ozone into the polar lower stratosphere.

This suggests that the radiative impact of the Cerro Hudson aerosol layer strengthens the cap against tropospheric wave activity entering the stratosphere, resulting in a colder, lower ozone collar region above 20km and above the layer of Cerro Hudson aerosols.

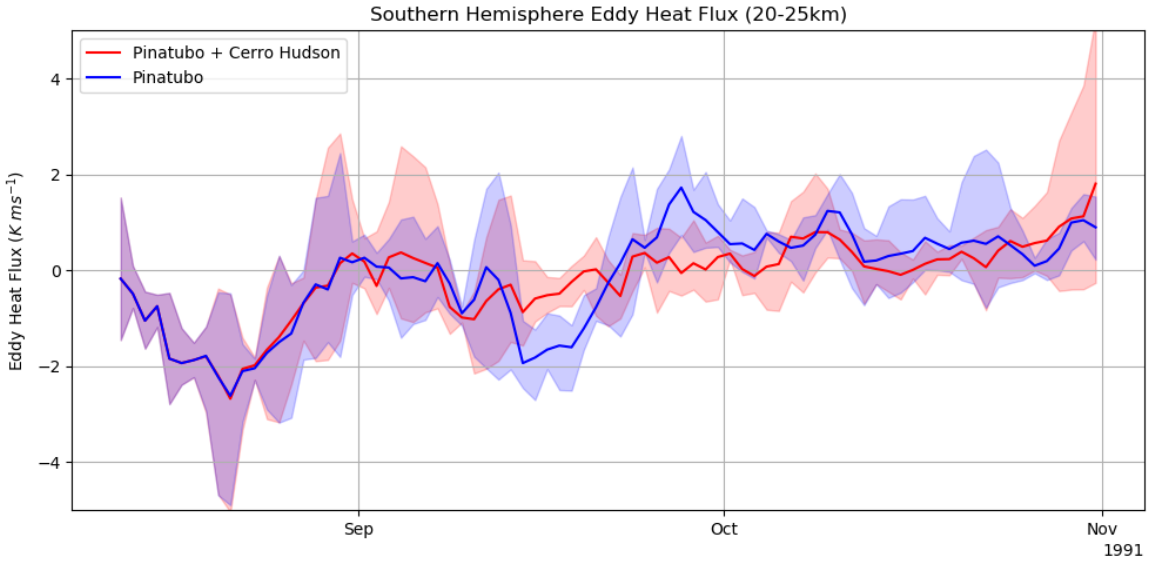

Figure 3.7: Southern hemisphere eddy heat flux in each ensemble plus the ensemble spread (shaded area) for the ensemble with Cerro Hudson (red) and the ensemble without Cerro Hudson (blue).

To further explain the dynamical difference between the ensembles, Fig. 3.8 shows the evolution of the poleward temperature gradient and vortex wind speed in the Southern Hemisphere in each ensemble. Following the eruption of Cerro Hudson, an increased temperature gradient at the altitude of the Antarctic vortex is associated with the stronger zonal wind which results in the longer-lasting isolated vortex later into the season seen in the ensemble including Cerro Hudson. Cerro Hudson aerosol, which remains in the midlatitudes radiatively heats the

stratosphere, increasing the poleward temperature gradient, causing a stronger thermal wind and more persistent vortex.

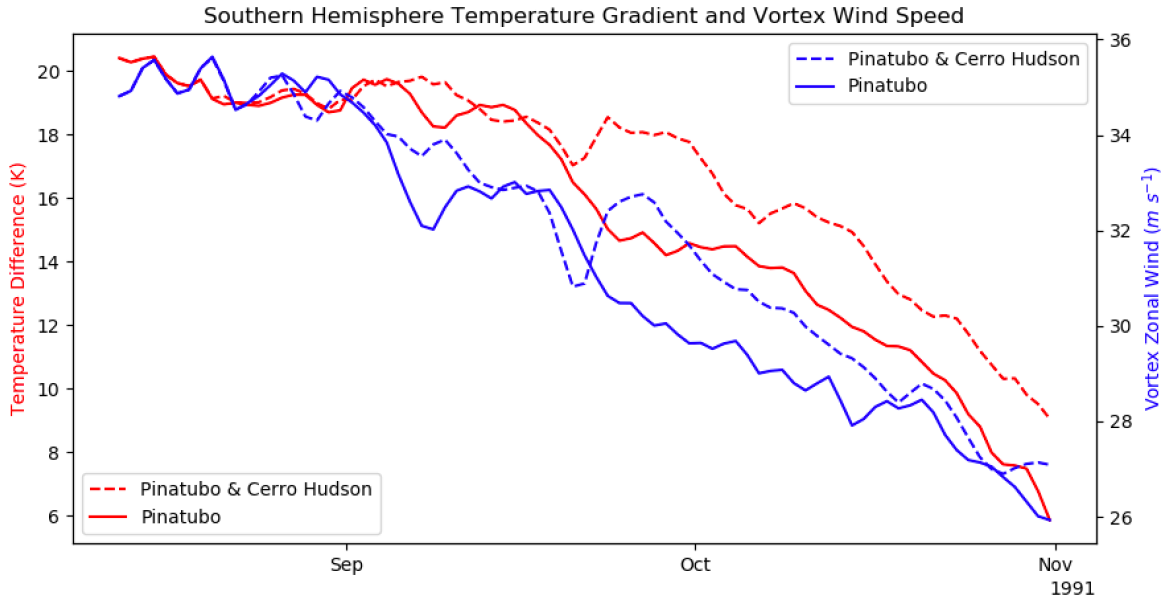

Figure 3.8: (Red) Southern hemisphere poleward temperature gradient, calculated as the temperature difference between the region between 15°S and 30°S and the region between 60°S and 90°S, both between 10 and 30 km. (Blue) Southern hemisphere vortex zonal wind speed. For each, the ensemble including both eruptions is shown as dashed lines while the ensemble only including Pinatubo is shown as a solid line.

3.4 Conclusions

The free-running GEOS/GC/CARMA model shows that the direct radiative impact of the August 15, 1991 Cerro Hudson eruption likely altered the dynamics of the Southern Hemisphere, heating the stratosphere at low latitudes, increasing the temperature difference between the low latitudes and the pole, strengthening the vortex, and suppressing tropospheric wave propagation into the stratosphere. This resulted in a slower breakdown of the Antarctic vortex than would have otherwise occurred. The dynamical forcing of the lower-stratospheric volcanic sulfate aerosols

resulting from the eruption in the model result in low ozone anomalies within the collar region in late September and October above 20 km. This ozone deficit results in higher ozone hole area relative to both the background and the ensemble excluding the Cerro Hudson eruption. While this dynamical impact is consistent across all ensemble members in this study, a larger ensemble is needed to validate this hypothesis. The GEOS/GC/CARMA model does include a coupling between the volcanic aerosols and chlorine and bromine activation, but we see little evidence that the aerosols from Pinatubo or Cerro Hudson significantly change the ozone chemistry of the 1991 Antarctic vortex above 20 km where there is little Cerro Hudson aerosol present. However, the model also predicts ozone loss below 15 km, where surface area in the model is increased in the collar region of the vortex by more than an order of magnitude. Cerro Hudson aerosol were below the primary, PSC-driven ozone depletion region where it may have caused a small additional ozone decrease. Combining the dynamical effect and the direct impact on chemistry, column ozone in this region was decreased in the model by a total of 12 DU and the size of the ozone hole increased by an average of 9% in October. Between 20 km and 25 km, local ozone is decreased by an average of 1.3 DU/km (0.37 ppmv) in October, an 11% decrease from background levels. The region between 15 km and 20 km in the model shows a decrease of 1.5 DU/km (0.11 ppmv), a 26% decrease from background levels. Ozone in this region was observed to decrease by 50% by Deshler et al., 1992 and this loss is consistent with both the satellite observations of ozone

from late September through October 1991 (Kreuger et al., 1992) as well as the in-situ aerosol and ozone measurements of Hofmann et al., 1992.

Finally, the shown impact of the Cerro Hudson eruption is deeply convolved with the impact of the 1991 eruption of Pinatubo, which happened two months prior. Figs. 6 and 7 show that the ensembles, both of which include Pinatubo, show an anomalously cold and persistent vortex prior to the impact of Cerro Hudson in late September. In the collar region specifically, ozone concentrations were 2.5 DU/km (0.71 ppmv) lower than the background and had recovered to background values from the Pinatubo-caused anomaly between 20km and 25 km by October 16th while the ensemble including Cerro Hudson recovered by October 30th weeks later on average. A similar lag is seen between 15 km and 20 km. Temperature in the collar region in August is 7.8 K colder in both ensembles when compared to background values. We have focused here on the impact on the 1991 ozone hole but the increasing aerosol surface area in the collar region in Fig. 3.6 show that the Pinatubo aerosols may have impacted the ozone hole in subsequent years, as has been shown by modeling and observational studies [Hofmann et al., 1993; Knight et al., 1998; Stenchikov et al., 2002].

BIBLIOGRAPHY

Angell, J.K., 1997. Stratospheric warming due to Agung, El Chichón, and Pinatubo taking into account the quasi-biennial oscillation. *Journal of Geophysical Research: Atmospheres*, *102*(D8), pp.9479-9485.

Aquila, V., Baldwin, C., Mukherjee, N., Hackert, E., Li, F., Marshak, J., Molod, A. and Pawson, S., 2021. Impacts of the Eruption of Mount Pinatubo on Surface Temperatures and Precipitation Forecasts With the NASA GEOS Subseasonal-to-Seasonal System. *Journal of Geophysical Research: Atmospheres*, *126*(16), p.e2021JD034830.

Aquila, V., Oman, L.D., Stolarski, R., Douglass, A.R. and Newman, P.A., 2013. The response of ozone and nitrogen dioxide to the eruption of Mt. Pinatubo at southern and northern midlatitudes. *Journal of the Atmospheric Sciences*, *70*(3), pp.894-900.

Aquila, V., Oman, L.D., Stolarski, R.S., Colarco, P.R. and Newman, P.A., 2012. Dispersion of the volcanic sulfate cloud from a Mount Pinatubo–like eruption. *Journal of Geophysical Research: Atmospheres*, *117*(D6).

Bardeen, C.G, O.B. Toon, E.J. Jensen, D.R. Marsh, and V.L. Harvey, 2008. Numerical simulations of the three-dimensional distribution of meteoric dust in the mesosphere and upper stratosphere. *Journal of Geophysical Research: Atmospheres, 113, D17202, doi:10.1029/2007JD009515.*

Bekki, S., 1995. Oxidation of volcanic SO_2: a sink for stratospheric OH and H_2O. *Geophysical Research Letters*, *22*(8), pp.913-916.

Bekki, S., Toumi, R. and Pyle, J.A., 1993. Role of sulphur photochemistry in tropical ozone changes after the eruption of Mount Pinatubo. *Nature*, *362*(6418), pp.331-333.

Bey, I., Jacob, D.J., Yantosca, R.M., Logan, J.A., Field, B.D., Fiore, A.M., Li, Q., Liu, H.Y., Mickley, L.J. and Schultz, M.G., 2001. Global modeling of tropospheric chemistry with assimilated meteorology: Model description and evaluation. *Journal of Geophysical Research: Atmospheres*, *106*(D19), pp.23073-23095.

Bluth, G.J., Doiron, S.D., Schnetzler, C.C., Krueger, A.J. and Walter, L.S., 1992. Global tracking of the SO_2 clouds from the June, 1991 Mount Pinatubo eruptions. *Geophysical Research Letters*, *19*(2), pp.151-154.

Carn, S.A., Clarisse, L. and Prata, A.J., 2016. Multi-decadal satellite measurements of global volcanic degassing. *Journal of Volcanology and Geothermal Research*, *311*, pp.99-134.

Chen, Z., Bhartia, P.K., Loughman, R., Colarco, P. and DeLand, M., 2018. Improvement of stratospheric aerosol extinction retrieval from OMPS/LP using a new aerosol model. *Atmospheric measurement techniques*, *11*(12), pp.6495-6509.

Colarco, P.R., Nowottnick, E.P., Randles, C.A., Yi, B., Yang, P., Kim, K.M., Smith, J.A. and Bardeen, C.G., 2014. Impact of radiatively interactive dust aerosols in the NASA GEOS-5 climate model: Sensitivity to dust particle shape and refractive index. *Journal of Geophysical Research: Atmospheres*, *119*(2), pp.753-786.

Constantine, E. K., Bluth, G. J., & Rose, W. I. (2000). TOMS and AVHRR observations of drifting volcanic clouds from the August 1991 eruptions of Cerro Hudson.

Washington DC American Geophysical Union Geophysical Monograph Series, *116*, 45-64.

Crutzen, P.J., 2006. Albedo enhancement by stratospheric sulfur injections: a contribution to resolve a policy dilemma?. *Climatic change*, *77*(3-4), p.211.

Deshler, T., Luo, B., Kovilakam, M., Peter, T. and Kalnajs, L.E., 2019. Retrieval of aerosol size distributions from in situ particle counter measurements: Instrument counting efficiency and comparisons with satellite measurements. *Journal of Geophysical Research: Atmospheres*, *124*(9), pp.5058-5087.

Dhomse, S.S., Chipperfield, M.P., Feng, W., Hossaini, R., Mann, G.W. and Santee, M.L., 2015. Revisiting the hemispheric asymmetry in midlatitude ozone changes following the Mount Pinatubo eruption: A 3-D model study. *Geophysical Research Letters*, *42*(8), pp.3038-3047.

Dhomse, S.S., Emmerson, K.M., Mann, G.W., Bellouin, N., Carslaw, K.S., Chipperfield, M.P., Hommel, R., Abraham, N.L., Telford, P., Braesicke, P. and Dalvi, M., 2014. Aerosol microphysics simulations of the Mt. Pinatubo eruption with the UM-UKCA composition-climate model. *Atmospheric Chemistry and Physics*, *14*(20), pp.11221-11246.

Doiron, S. D., Bluth, G. J., Schnetzler, C. C., Krueger, A. J., & Walter, L. S. (1991). Transport of Cerro Hudson SO2 clouds. *Eos, Transactions American Geophysical Union*, *72*(45), 489-498.

Douglass, A. R., R. S. Stolarski, S. E. Strahan, and L. D. Oman, 2012. Understanding differences in upper stratospheric ozone response to changes in chlorine and temperature as computed using CCMVal-2 models. *Journal of Geophysical Research: Atmospheres*, *117, D16306, doi:10.1029/2012JD017483.*

Dutton, E.G. and Christy, J.R., 1992. Solar radiative forcing at selected locations and evidence for global lower tropospheric cooling following the eruptions of El Chichón and Pinatubo. *Geophysical research letters*, *19*(23), pp.2313-2316.

English, J.M., Toon, O.B. and Mills, M.J., 2013. Microphysical simulations of large volcanic eruptions: Pinatubo and Toba. *Journal of Geophysical Research: Atmospheres*, *118*(4), pp.1880-1895.

Free, M. and Lanzante, J., 2009. Effect of volcanic eruptions on the vertical temperature profile in radiosonde data and climate models. *Journal of climate*, *22*(11), pp.2925-2939.

Guo, S., Bluth, G.J., Rose, W.I., Watson, I.M. and Prata, A.J., 2004. Re-evaluation of SO_2 release of the 15 June 1991 Pinatubo eruption using ultraviolet and infrared satellite sensors. *Geochemistry, Geophysics, Geosystems*, *5*(4).

Hill, C., DeLuca, C., Suarez, M. and Da Silva, A., 2004. The architecture of the earth system modeling framework. *Computing in Science & Engineering*, *6*(1), pp.18-28.

Hofmann, D.J. and Oltmans, S.J., 1993. Anomalous Antarctic ozone during 1992: Evidence for Pinatubo volcanic aerosol effects. *Journal of Geophysical Research: Atmospheres*, *98*(D10), pp.18555-18561.

Holasek, R.E., Self, S. and Woods, A.W., 1996. Satellite observations and interpretation of the 1991 Mount Pinatubo eruption plumes. *Journal of Geophysical Research: Solid Earth*, *101*(B12), pp.27635-27655.

Janssens-Maenhout, G., Crippa, M., Guizzardi, D., Dentener, F., Muntean, M., Pouliot, G., Keating, T., Zhang, Q., Kurokawa, J., Wankmüller, R. and Denier van der Gon, H., 2015. HTAP_v2. 2: a mosaic of regional and global emission grid maps for 2008 and 2010 to study hemispheric transport of air pollution. *Atmospheric Chemistry and Physics*, *15*(19), pp.11411-11432.

Kerr, R.A., 1993. Ozone takes a nose dive after the eruption of Mt. Pinatubo. *Science*, *260*(5107), pp.490-491.

Kinne, S., Toon, O.B. and Prather, M.J., 1992. Buffering of stratospheric circulation by changing amounts of tropical ozone a Pinatubo Case Study. *Geophysical research letters*, *19*(19), pp.1927-1930.

Knight, J.R., Austin, J., Grainger, R.G. and Lambert, A., 1998. A three-dimensional model simulation of the impact of Mt. Pinatubo aerosol on the Antarctic ozone hole. *Quarterly Journal of the Royal Meteorological Society*, *124*(549), pp.1527-1558.

Kovilakam, M., Thomason, L.W., Ernest, N., Rieger, L., Bourassa, A. and Millán, L., 2020. The global space-based stratospheric aerosol climatology (version 2.0): 1979–2018. *Earth System Science Data*, *12*(4), pp.2607-2634.

Kovilakam, M., Thomason, L.W., Ernest, N., Rieger, L., Bourassa, A. and Millán, L., 2020. The global space-based stratospheric aerosol climatology (version 2.0): 1979–2018. *Earth System Science Data*, *12*(4), pp.2607-2634.

Krueger, A., Schoeberl, M., Newman, P., & Stolarski, R. (1992). The 1991 Antarctic ozone hole; TOMS observations. *Geophysical research letters*, *19*(12), 1215-1218.

Kravitz, B., MacMartin, D.G., Mills, M.J., Richter, J.H., Tilmes, S., Lamarque, J.F., Tribbia, J.J. and Vitt, F., 2017. First simulations of designing stratospheric sulfate aerosol geoengineering to meet multiple simultaneous climate objectives. *Journal of Geophysical Research: Atmospheres*, *122*(23), pp.12-616.

Kremser, S., Thomason, L.W., von Hobe, M., Hermann, M., Deshler, T., Timmreck, C., Toohey, M., Stenke, A., Schwarz, J.P., Weigel, R. and Fueglistaler, S., 2016. Stratospheric aerosol—Observations, processes, and impact on climate. *Reviews of Geophysics*, *54*(2), pp.278-335.

LeGrande, A.N., Anchukaitis, K.J., von Gunten, L. and Goodwin, L. eds., 2015. *Volcanoes and climate*. PAGES International Project Office.

Long, C.S. and Stowe, L.L., 1994. Using the NOAA/AVHRR to study stratospheric aerosol optical thicknesses following the Mt. Pinatubo eruption. *Geophysical research letters*, *21*(20), pp.2215-2218.

MacMartin, D.G., Kravitz, B., Tilmes, S., Richter, J.H., Mills, M.J., Lamarque, J.F., Tribbia, J.J. and Vitt, F., 2017. The climate response to stratospheric aerosol geoengineering can be tailored using multiple injection locations. *Journal of Geophysical Research: Atmospheres*, *122*(23), pp.12-574.

McCormick, M.P., Thomason, L.W. and Trepte, C.R., 1995. Atmospheric effects of the Mt Pinatubo eruption. *Nature*, *373*(6513), pp.399-404.

McKeen, S.A., Liu, S.C. and Kiang, C.S., 1984. On the chemistry of stratospheric SO_2 from volcanic eruptions. *Journal of Geophysical Research: Atmospheres*, *89*(D3), pp.4873-4881.

Miles, G. M., Siddans, R., Grainger, R. G., Prata, A. J., Fisher, B., & Krotkov, N. (2017). Retrieval of volcanic SO_2 from HIRS/2 using optimal estimation. *Atmospheric Measurement Techniques*, *10*(7), 2687-2702.

Mills, M.J., Richter, J.H., Tilmes, S., Kravitz, B., MacMartin, D.G., Glanville, A.A., Tribbia, J.J., Lamarque, J.F., Vitt, F., Schmidt, A. and Gettelman, A., 2017. Radiative and chemical response to interactive stratospheric sulfate aerosols in fully coupled CESM1 (WACCM). *Journal of Geophysical Research: Atmospheres*, *122*(23), pp.13-061.

Mills, M.J., Schmidt, A., Easter, R., Solomon, S., Kinnison, D.E., Ghan, S.J., Neely III, R.R., Marsh, D.R., Conley, A., Bardeen, C.G. and Gettelman, A., 2016. Global volcanic aerosol properties derived from emissions, 1990–2014, using CESM1 (WACCM). *Journal of Geophysical Research: Atmospheres*, *121*(5), pp.2332-2348.

Molod, A., Takacs, L., Suarez, M. and Bacmeister, J., 2015. Development of the GEOS-5 atmospheric general circulation model: Evolution from MERRA to MERRA2. *Geoscientific Model Development*, *8*(5), pp.1339-1356.

Neely III, R.R., Toon, O.B., Solomon, S., Vernier, J.P., Alvarez, C., English, J.M., Rosenlof, K.H., Mills, M.J., Bardeen, C.G., Daniel, J.S. and Thayer, J.P., 2013. Recent anthropogenic increases in SO_2 from Asia have minimal impact on stratospheric aerosol. *Geophysical Research Letters*, *40*(5), pp.999-1004.

Niemeier, U., Timmreck, C., Graf, H.F., Kinne, S., Rast, S. and Self, S., 2009. Initial fate of fine ash and sulfur from large volcanic eruptions. *Atmospheric Chemistry and Physics*, *9*(22), pp.9043-9057.

Pitari, G., Di Genova, G., Mancini, E., Visioni, D., Gandolfi, I. and Cionni, I., 2016. Stratospheric aerosols from major volcanic eruptions: A composition-climate model study of the aerosol cloud dispersal and e-folding time. *Atmosphere*, *7*(6), p.75.

Prather, M., 1992. Catastrophic loss of stratospheric ozone in dense volcanic clouds. *Journal of Geophysical Research: Atmospheres*, *97*(D9), pp.10187-10191.

Santer, B.D., Bonfils, C., Painter, J.F., Zelinka, M.D., Mears, C., Solomon, S., Schmidt, G.A., Fyfe, J.C., Cole, J.N., Nazarenko, L. and Taylor, K.E., 2014. Volcanic contribution to decadal changes in tropospheric temperature. *Nature Geoscience*, *7*(3), pp.185-189.

Schoeberl, M. R., Doiron, S. D., Lait, L. R., Newman, P. A., & Krueger, A. J. (1993). A simulation of the Cerro Hudson SO2 cloud. *Journal of Geophysical Research: Atmospheres*, *98*(D2), 2949-2955.

Solomon, S., 1999. Stratospheric ozone depletion: A review of concepts and history. *Reviews of Geophysics*, *37*(3), pp.275-316.

Solomon, S., Ivy, D.J., Kinnison, D., Mills, M.J., Neely III, R.R. and Schmidt, A., 2016. Emergence of healing in the Antarctic ozone layer. *Science*, *353*(6296), pp.269-274.

Stenchikov, G.L., Kirchner, I., Robock, A., Graf, H.F., Antuña, J.C., Grainger, R.G., Lambert, A. and Thomason, L., 1998. Radiative forcing from the 1991 Mount Pinatubo volcanic eruption. *Journal of Geophysical Research: Atmospheres*, *103*(D12), pp.13837-13857.

Stenchikov, G., Ukhov, A., Osipov, S., Ahmadov, R., Grell, G., Cady-Pereira, K., Mlawer, E. and Iacono, M., 2021. How Does a Pinatubo-Size Volcanic Cloud Reach the

Middle Stratosphere?. *Journal of Geophysical Research: Atmospheres*, *126*(10), p.e2020JD033829.
Stone, K.A., Solomon, S., Kinnison, D.E., Pitts, M.C., Poole, L.R., Mills, M.J., Schmidt, A., Neely III, R.R., Ivy, D., Schwartz, M.J. and Vernier, J.P., 2017. Observing the impact of Calbuco volcanic aerosols on South Polar ozone depletion in 2015. *Journal of Geophysical Research: Atmospheres*, *122*(21), pp.11-862.
Sukhodolov, T., Sheng, J.X., Feinberg, A., Luo, B.P., Peter, T., Revell, L., Stenke, A., Weisenstein, D.K. and Rozanov, E., 2018. Stratospheric aerosol evolution after Pinatubo simulated with a coupled size-resolved aerosol–chemistry–climate model, SOCOL-AERv1. 0. *Geoscientific Model Development*, *11*(7), pp.2633-2647.
Tabazadeh, A., Drdla, K., Schoeberl, M.R., Hamill, P. and Toon, O.B., 2002. Arctic "ozone hole" in a cold volcanic stratosphere. *Proceedings of the National Academy of Sciences*, *99*(5), pp.2609-2612.
Tilmes, S., Richter, J.H., Kravitz, B., MacMartin, D.G., Mills, M.J., Simpson, I.R., Glanville, A.S., Fasullo, J.T., Phillips, A.S., Lamarque, J.F. and Tribbia, J., 2018. CESM1 (WACCM) stratospheric aerosol geoengineering large ensemble project. *Bulletin of the American Meteorological Society*, *99*(11), pp.2361-2371.
Timmreck, C., Graf, H.F. and Kirchner, I., 1999. A one and half year interactive MA/ECHAM4 simulation of Mount Pinatubo Aerosol. *Journal of Geophysical Research: Atmospheres*, *104*(D8), pp.9337-9359.
Toon, O.B., Turco, R.P., Westphal, D., Malone, R. and Liu, M., 1988. A multidimensional model for aerosols: Description of computational analogs. *Journal of Atmospheric Sciences*, *45*(15), pp.2123-2144.
Tupper, A., Oswalt, J.S. and Rosenfeld, D., 2005. Satellite and radar analysis of the volcanic-cumulonimbi at Mount Pinatubo, Philippines, 1991. *Journal of Geophysical Research: Atmospheres*, *110*(D9).
Visioni, D., MacMartin, D.G., Kravitz, B., Tilmes, S., Mills, M.J., Richter, J.H. and Boudreau, M.P., 2019. Seasonal injection strategies for stratospheric aerosol geoengineering. *Geophysical Research Letters*, *46*(13), pp.7790-7799.
Yang, W., Vecchi, G.A., Fueglistaler, S., Horowitz, L.W., Luet, D.J., Muñoz, Á.G., Paynter, D. and Underwood, S., 2019. Climate impacts from large volcanic eruptions in a high-resolution climate model: The importance of forcing structure. *Geophysical Research Letters*, *46*(13), pp.7690-7699.
Zhu, Y., Toon, O.B., Jensen, E.J., Bardeen, C.G., Mills, M.J., Tolbert, M.A., Yu, P. and Woods, S., 2020. Persisting volcanic ash particles impact stratospheric SO2 lifetime and aerosol optical properties. *Nature communications*, *11*(1), pp.1-11.
Zhu, Y., Toon, O.B., Kinnison, D., Harvey, V.L., Mills, M.J., Bardeen, C.G., Pitts, M., Bègue, N., Renard, J.B., Berthet, G. and Jégou, F., 2018. Stratospheric aerosols, polar stratospheric clouds, and polar ozone depletion after the Mount Calbuco eruption in 2015. *Journal of Geophysical Research: Atmospheres*, *123*(21), pp.12-308.

APPENDIX

A.1 Nucleation in CARMA

CARMA uses a binary homogeneous nucleation scheme based on Zhao & Turco, 1995 with a few improvements. First, following the method of Tabazadeh (1997) the model calculates equilibrium vapor pressure of H_2O and H_2SO_4 over an aqueous solution of w percent sulfuric acid by weight (Giauque et al., 1960). The model corrects for changes in the latent heat of vaporization with changes in temperature according to Kulmala and Laaksonen (1990). These vapor pressures are calculated and stored in a lookup table. Based on this lookup table, CARMA calculates the weight percent with minimum Gibbs Free Energy according to Zhao & Turco:

$$\Delta\mu_1\left[1+\frac{\mathrm{d}\ln\rho}{\mathrm{d}\omega}\omega\right]-\frac{M_1}{M_2}\Delta\mu_2\left[1-\frac{\mathrm{d}\ln\rho}{\mathrm{d}\omega}(1-\omega)\right]=0,$$

Based on this "critical weight percent", the radius, Gibbs Free Energy, and finally nucleation rate is calculated. The method for calculating nucleation rate is the same as Zhao & Turco except that a Zeldovich factor, Z, is included.

$$J_{hom} = 4\pi(r^*)^2 N_2 \beta_1 Z\, exp(-\frac{\Delta G^*_{hom}}{k_B T})$$

The Zeldovich factor represents the depletion of molecular clusters relative to equilibrium near the critical size due to ongoing nucleation (Jaecker-Voirol & Mirabel, 1988).

A.2 Condensational Growth and Evaporation in CARMA

Growth in the aerosol continuity equation is given as

$$\frac{dC(v)}{dt} = -\frac{dC(v)g(v)}{dr}$$

where C(v) is the concentration of particles per volume of air and g(v) is the particle growth or evaporation rate. CARMA calculates g(v) according to the method laid out in the appendix of Toon et al., 1989:

$$dr/dt \;=\; g_0 n_{vap}[S \;-\; A_k(1+g_1 g_2 Q_{rad})]/[1+g_1 g_0 n_\infty]$$

where n_{vap} is the vapor pressure of sulfuric acid expressed as a number density, n_∞ is the number concentration of sulfuric acid molecules in the gas phase, $S = \frac{n_\infty}{n_{vap}}$ is the saturation ratio, $A_k$is the Kelvin term, Q_{rad} is the rate of radiative heating (here assumed to be zero), n_∞ is the number concentration of vapor molecules far from the surface, and

$$g_0 = DF_v M/r\rho A$$
$$g_1 = {L_e}^2 M\rho r/RT_\infty K F_t$$
$$g_2 = 1/L_e 4\pi r^2 \rho$$

where $F_v$and F_t are ventilation corrections, L_e is the latent heat of sublimation, T_∞ is the temperature far from the particle, ρ is the density of the particle, M is the

molecular weight of water, D is the diffusion coefficient, and K is thermal conductivity (Toon et al., 1989). F_v and F_t represent corrections for the effects of sedimentation of the particles on the flux of water vapor molecules and heat to and from the particles, respectively. These factors are calculated with the functions recommended by Pruppacher and Klett (1978). D and K are calculated with the forms from Fuchs and Sutugin, 1971:

$$D = D'C/(r + \lambda CKn_d/\phi_0)$$
$$K = K'C/(r + \lambda CKn_d/\phi_0)$$

where Kn is the Knudsen number, D' is the temperature dependent diffusivity of water in air, and K' is the thermal conductivity of air, C is a correction for the shape of particles at small Knudsen numbers. Once a growth rate has been calculated, CARMA uses the piecewise parabolic method (PPM) to calculate the flux of particles across each mass bin boundary (Colella and Woodward, 1984).

A.3 Coagulation in CARMA

Coagulation is described in the aerosol continuity equation by:

$$\frac{dC(v)}{dt} = \frac{1}{2}\int_0^v K_c(u, v-u)C(u)C(v-u)du \; - \; C(v)\int_0^\infty K_c(u,v)C(u)du$$

where K_c is the coagulation kernel. CARMA calculates the coagulation using the numerical approach of Jacobson et al., 1994. The Brownian diffusion kernel used is from Fuchs, 1964:

$$K_c(i,j) = \frac{4\pi(r_i + r_j)(D_i + D_j)}{\dfrac{r_i + r_j}{r_i + r_j + ({\delta_i}^2 + {\delta_j}^2)^{1/2}} + \dfrac{4(D_i + D_j)}{({v_{pi}}^2 + {v_{pj}}^2)^{1/2}(r_i + r_j)}}$$

where r_i and r_j are the radii of two particles, v_{pi} and v_{pj} are the velocities of the particles, $\delta_i$and δ_j are the mean distance reached by particles leaving the surface of the particle, D_i and D_j are the particle diffusion coefficient given by

$$D_i = \frac{k_B T}{6\pi r_i \eta}\{1 + K_n[A + B\, exp(-C{K_n}^{-1})]\}$$

where $K_n = \lambda/r$ is the Knudsen number of the particle, k_B is the Boltzmann constant, T is the temperature, η is the dynamic viscosity of air, and A, B, and C are constants for correcting for particle resistance to motion (Jacobson et al., 1994).

A.4 Particle Settling in CARMA

Particle settling is represented in the aerosol continuity equation by

$$\frac{dC(v)}{dt} = -\frac{d([W + V_{fall}\, C(v))}{dz}$$

where W is the vertical wind speed, V_{fall} is the fall velocity, and C(v) is the concentration of particles per volume of air. GEOS-5's dynamical core (Lin, 2004) solves vertical transport by remapping the model's vertical layers instead of explicitly calculating W, meaning settling is decoupled from large-scale vertical

transport. Aerosol fall velocity (V_f) is calculated according to Stokes-Cunningham theory using slip and mobility corrections:

$$V_f = \frac{2\rho_p g r^2}{9\mu_a}$$

where ρ_p is the density of the particle, μ_a is density of the air times the vertical velocity of the air, g is the gravitational constant, and r is the aerodynamic the radius of the particle (Pruppacher and Klett, 1978).